Repeated pulses of vertical methane flux recorded in glacial sediments from the southeast Bering Sea

Mea S. Cook,[1] Lloyd D. Keigwin,[2] Daniel Birgel,[3,4] and Kai-Uwe Hinrichs[3]

Received 19 May 2010; revised 3 January 2011; accepted 25 January 2011; published 11 May 2011.

[1] There is controversy over the role of marine methane hydrates in atmospheric methane concentrations and climate change during the last glacial period. In this study of two sediment cores from the southeast Bering Sea (700 m and 1467 m water depth), we identify multiple episodes during the last glacial period of intense methane flux reaching the seafloor. Within the uncertainty of the radiocarbon age model, the episodes are contemporaneous in the two cores and have similar timing and duration as Dansgaard-Oeschger events. The episodes are marked by horizons of sediment containing ^{13}C-depleted authigenic carbonate minerals; ^{13}C-depleted archaeal and bacterial lipids, which resemble those found in ANME-1 type anaerobic methane oxidizing microbial consortia; and changes in the abundance and species distribution of benthic foraminifera. The similar timing and isotopic composition of the authigenic carbonates in the two cores is consistent with a region-wide increase in the upward flux of methane bearing fluids. This study is the first observation outside Santa Barbara Basin of pervasive, repeated methane flux in glacial sediments. However, contrary to the "Clathrate Gun Hypothesis" (Kennett et al., 2003), these coring sites are too deep for methane hydrate destabilization to be the cause, implying that a much larger part of the ocean's sedimentary methane may participate in climate or carbon cycle feedback at millennial timescales. We speculate that pulses of methane in these opal-rich sediments could be caused by the sudden release of overpressure in pore fluids that builds up gradually with silica diagenesis. The release could be triggered by seismic shaking on the Aleutian subduction zone caused by hydrostatic pressure increase associated with sea level rise at the start of interstadials.

Citation: Cook, M. S., L. D. Keigwin, D. Birgel, and K.-U. Hinrichs (2011), Repeated pulses of vertical methane flux recorded in glacial sediments from the southeast Bering Sea, *Paleoceanography*, *26*, PA2210, doi:10.1029/2010PA001993.

1. Introduction

[2] The dynamics of methane in the ocean-atmosphere system in the late Pleistocene is controversial. There is geochemical evidence of episodic methane release from sediments from several ocean basins during the last glacial period (Figure 1), but whether these happen simultaneously or are important to atmospheric budgets is unclear. Isotopic analyses of methane in fossil air samples from Greenland ice cores do not support the hypothesis that sedimentary methane is solely responsible for elevated atmospheric concentration at millennial time scales during the relatively warm climate intervals of the last glacial period and deglaciation [*Bock et al.*, 2010; *Petrenko et al.*, 2009; *Schaefer et al.*, 2006; *Sowers*, 2006]. However, the reservoir of methane in marine sediments is so large, a perturbation has the potential to significantly affect the atmospheric methane budget and climate, whether or not release of methane is globally synchronized.

[3] After water vapor and carbon dioxide, methane is the greenhouse gas responsible for the greatest greenhouse warming of the atmosphere [*Solomon et al.*, 2007]. The preindustrial reservoir of atmospheric methane is 760 ppbv, or 2200 Tg [*Lelieveld et al.*, 1993]. Though the modern methane budget is not completely constrained, the natural flux of methane to the atmosphere is dominated by wetlands at 92–232 Tg CH_4 year^{-1}, and the flux from marine sediments is estimated at 0.4–12.2 Tg CH_4 year^{-1} [*Wuebbles and Hayhoe*, 2002]. The reservoirs of methane in seafloor sediments are estimated at 2,100,000–2,700,000 Tg CH_4 [*Archer*, 2009], three orders of magnitude larger than the atmospheric reservoir.

[4] Release of methane from seafloor sediments is thought to be associated with climate changes in the past, including

[1]Geosciences Department, Williams College, Williamstown, Massachusetts, USA.
[2]Geology and Geophysics Department, Woods Hole Oceanographic Institution, Woods Hole, Massachusetts, USA.
[3]MARUM-Center for Marine Environmental Sciences, University of Bremen, Bremen, Germany.
[4]Now at Department of Geodynamics and Sedimentology, University of Vienna, Vienna, Austria.

0883-8305/11/2010PA001993

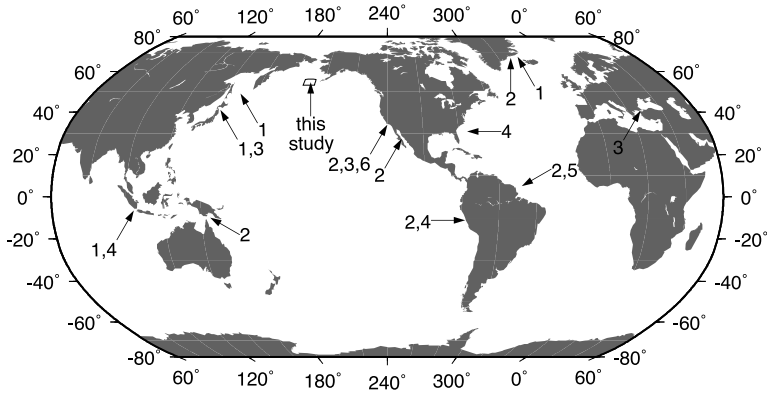

Figure 1. Location of marine sediment cores with geological evidence of methane seepage during the last glacial cycle. (1) Authigenic carbonates with low δ^{13}C [*Hoshiba et al.*, 2006; *Lembke et al.*, 2004; *Millo et al.*, 2005; *Wiedicke and Weiss*, 2006]; (2) foraminifera tests with low δ^{13}C [*de Garidel-Thoron et al.*, 2004; *Keigwin*, 2002; *Kennett et al.*, 2000; *Maslin et al.*, 2005; *Smith et al.*, 2001; *Wefer et al.*, 1994]; (3) biomarkers of methanotrophy [*Hinrichs et al.*, 2003; *Ménot and Bard*, 2010; *Uchida et al.*, 2004b]; (4) benthic foraminifer assemblage characteristic of methane seep sites [*Bhaumik and Gupta*, 2007; *Wefer et al.*, 1994; *Wiedicke and Weiss*, 2006]; (5) slope failure associated with methane release from sediments [*Maslin et al.*, 1998; *Maslin et al.*, 2005]; and (6) tar, asphalt seepage [*Hill et al.*, 2006; *Valentine et al.*, 2010].

the early Jurassic [*Hesselbo et al.*, 2000], the late Paleocene thermal maximum [*Dickens et al.*, 1995], and in the last glacial period [*Kennett et al.*, 2003]. In the late Pleistocene, atmospheric methane varied between 350 and 760 ppbv, or 1010 and 2200 Tg, where methane is high during warm interglacial periods, and low during cold glacial periods [*Chappellaz et al.*, 1990; *Loulergue et al.*, 2008]. During the last glacial period, warm, interstadial climate episodes [*Johnsen et al.*, 1992] known as Dansgaard-Oeschger (D-O) oscillations were associated with elevated atmospheric methane concentrations [*Blunier et al.*, 1998]. Higher levels of methane during warm climate phases are thought to have resulted from expanded wetlands [*Chappellaz et al.*, 1990]. However, *Kennett et al.* [2003] proposed that sedimentary methane hydrates could be a significant source of atmospheric methane during D-O events, if slope waters at many locations warmed enough to destabilize methane hydrates.

[5] Evidence of methane flux from the seafloor during the late Quaternary comes from Santa Barbara Basin [*Hill et al.*, 2006; *Hinrichs et al.*, 2003; *Kennett et al.*, 2000; *Valentine et al.*, 2010], the Gulf of California [*Keigwin*, 2002], the Japan margin [*Hoshiba et al.*, 2006; *Uchida et al.*, 2004a], the Okhotsk Sea [*Lembke et al.*, 2004], the Papua Gulf [*de Garidel-Thoron et al.*, 2004], the Indonesian margin [*Wiedicke and Weiss*, 2006], the Peru margin [*Wefer et al.*, 1994], the east Greenland shelf [*Smith et al.*, 2001], the southwest Greenland Sea [*Millo et al.*, 2005], Blake Ridge [*Bhaumik and Gupta*, 2007], the Amazon Fan [*Maslin et al.*, 1998; *Maslin et al.*, 2005], and the sea of Marmara [*Ménot and Bard*, 2010]. The geological records of methane flux out of sediments (Figure 1) include indirect markers for the presence of methane seeps such as the presence of authigenic carbonate minerals with low δ^{13}C [*Peckmann and Thiel*, 2004], assemblages of benthic foraminifera typical of seep areas [e.g., *Bernhard et al.*, 2001], biomarkers of the microbial community that oxidizes methane [*Niemann and Elvert*, 2008], or presence of tar and asphalt emitted by a hydrocarbon seep along with methane [*Naehr et al.*, 2009]. It also includes the low-δ^{13}C signature of oxidized methane incorporated into the calcium carbonate tests of planktic and benthic foraminifera from dissolved inorganic carbon in seawater or pore water. Slope failures in the Amazon Fan are linked to methane release [*Maslin et al.*, 1998, 2005].

[6] The Bering Sea is a subpolar marginal basin with very productive surface waters and high delivery of organic carbon to sediments, especially along the Bering Slope [*Springer et al.*, 1996]. Evidence for biogenic sedimentary methane in the Bering Sea was first noted in the early days of ocean drilling [*Claypool et al.*, 1973; *Scholl et al.*, 1973], and more recently, gassy sediments and shallow sulfate-methane transition zones (6–10 mbsf) were observed during coring of the Umnak Plateau and Bering Slope regions during Leg 323 of the Integrated Ocean Drilling Program [*Takahashi et al.*, 2011].

[7] In this study of two cores from the southeast Bering Sea (Figure 2), we identify multiple episodes during the last glacial period of elevated methane flux. There are horizons of sediment containing both ^{13}C-depleted authigenic carbonate minerals and ^{13}C-depleted molecular fossils of consortia of anaerobic methane oxidizing archaea and sulfate reducing bacteria, and changes in the abundance and species distribution of benthic foraminifera. Since our sites are well within the gas hydrate stability zone, a mechanism other than hydrate destabilization must be responsible. Our observations are consistent with episodic region-wide increases in the upward flux of methane bearing fluids.

2. Methods

[8] Piston cores HLY02-02-51JPC (1467 m water depth) and HLY02-02-57JPC (700 m water depth) were collected in June 2002 from the crest of the broad spur between the Bering and Bristol canyons in the southeast Bering Sea (Figure 2). From CTD casts, bottom temperatures at the two coring sites are 2.2°C at 51JPC and 3.2°C at 57JPC. After

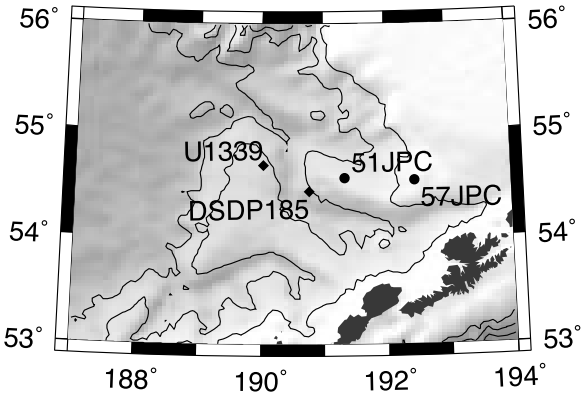

Figure 2. Map of the southeast Bering Sea showing the location of study areas HLY02-02-51JPC and 57JPC. The locations of DSDP 185 and IODP U1339 are also shown. Bathymetry is from *Smith and Sandwell* [1997], and contours are at 1 km intervals.

transport back to Woods Hole, the cores were split lengthwise and stored at 5°C. One centimeter thick samples were taken approximately every 8 cm from the core top to 1192 cm in 51JPC and from the core top to 1096 cm in 57JPC.

2.1. Micropaleontology

[9] We oven-dried sediment samples for foraminifer isotope analyses at 50°C, disaggregated them with tap water, washed them through a 63 μm sieve, then oven-dried them again. We picked the planktic foraminifer *Neogloboquadrina pachyderma* (sinistral) and the benthic foraminifer *Uvigerina peregrina* from the 150–250 μm and >250 μm size fractions, respectively. Without further cleaning, we analyzed samples consisting of 8–10 *N. pachyderma* (s.) or a single *U. peregrina* on a Finnigan MAT253 mass spectrometer with a Kiel device. We report the δ^{18}O and δ^{13}C relative to the VPDB standard [*Ostermann and Curry*, 2000]. We counted and identified benthic foraminifera from the >150 μm size fraction and calculated absolute abundance per gram dry sediment.

[10] After ultrasonic cleaning, we submitted samples of *N. pachyderma* (s.) to the National Ocean Sciences Accelerator Mass Spectrometer Facility at WHOI for AMS ^{14}C analysis. We measured the δ^{13}C either on an aliquot of the sample or measured on a separate sample from the same depth. The ^{14}C measurements (Table 1) were transformed to calendar ages using the Calib 6.0 software [*Stuiver and Reimer*, 1993; M. Stuiver et al., Calib calibration program, version 6.0, 2005]. We used the Marine09 calibration data set [*Reimer et al.*, 2009] and assumed that ΔR, the local anomaly of the age of surface water from the global mean, is constant at 400 years with an uncertainty of ±200 years [*Cook et al.*, 2005]. This corresponds to a total reservoir correction, $R + \Delta R$, of 800 ± 200 years.

[11] We made depth-age models for these cores assuming constant sediment accumulation rates between calibrated ^{14}C ages. After the cores were collected, cut into sections, and stored vertically, the sediment settled, leaving gaps between sections of up to 8 cm. Before linearly interpolating between radiocarbon dates, we placed the sediment data on a composite depth scale by concatenating core sections without the gaps. A tie point between the two cores (1138 cm in 51JPC to 1045 cm in 57JPC) is based on magnetic susceptibility (χ) and is used to put the deeper portion of 57JPC on an age scale (data not shown). The tie point is consistent with a detailed correlation between the two cores based on χ, natural remanent magnetism (NRM) and NRM inclination (S. P. Lund, unpublished data, 2010).

2.2. Lipid Biomarkers

[12] We took sediment samples for lipid extraction from the sediment cores in December 2006. We freeze-dried the samples with a Martin Christ Alpha 1–4 freeze dryer, then ground them with an agate mortar and pestle. We extracted 8–14 g of homogenized sediment with a mixture of dichloromethane and methanol (3:1 ratio) after addition of 20 μg of each of four internal standards, cholestane, behenic acid methyl ester, 1-nonadecanol and 2-methyl octadecanoic acid. For each extraction step, we used 4 mL of solvent per gram sample, and heated the mixture at 300 W to 80°C for 10 min in a CEM Mars X microwave solvent extraction system. We centrifuged the sample and decanted the supernatant, and repeated the extraction procedure three more times. We evaporated the solvent from the total lipid extract (TLE) under a stream of N_2 in a 35°C water bath (Turbovap II).

[13] We analyzed all compounds in the alcohol fraction as their trimethylsilyl (TMS) derivatives in a Thermo Electron Trace MS gas chromatograph–mass spectrometer (GC-MS) with a RTX-5MS fused-silica capillary column (30 m length, 0.25 mm inner diameter, 0.25 μm film thickness) using helium as the carrier gas. We used the following temperature program: injection at 60°C, isothermal for 2 min, heat at 10°C min^{-1} to 150°C, heat at 4°C min^{-1} to 320°C, isothermal for 31.5 min. We identified compounds based on their retention times and comparison to published mass spectra. In order to study the constituent biphytanes of glycerol dibiphytanyl glycerol tetraethers (GDGTs) and their compound-specific carbon isotopic compositions, we performed ether cleavage [*Hoefs et al.*, 1997] of an aliquot of the nonderivatized alcohol fraction after addition of 20 μg of 5α-cholestane as a recovery standard.

Table 1. Radiocarbon Measurements of *N. pachyderma* (s.) and Calibrated Ages

Depth (cm)	δ^{13}C (‰)	Conventional ^{14}C Age (years BP ± 1σ)	Calibrated ^{14}C Age[a] (cal BP ± 1σ)
	HLY02-02-57JPC		
87.5–88.5	−0.7[b]	15,500 ± 75	17,890 ± 570
255.5–256.5	0.1[b]	18,600 ± 75	21,200 ± 320
303.5–304.5	−18.2[c]	21,800 ± 110	not calibrated[d]
337.5–338.5	0.2[c]	20,800 ± 90	23,890 ± 320
405.5–408.5	−0.3[b]	21,500 ± 100	24,690 ± 280
	HLY02-02-51JPC		
134.5–135.5	−0.2[b]	10,600 ± 60	11,240 ± 390
177.5–178.5	−0.6[b]	12,500 ± 60	13,560 ± 200
241.5–242.5	−1.7[b]	14,050 ± 85	16,080 ± 560
479.5–480.5	−0.3[b]	18,200 ± 110	20,750 ± 370
543.5–544.5	−12.8[c]	20,700 ± 95	not calibrated[d]
664.5–666.5	−0.6[b]	21,600 ± 170	24,800 ± 350
1102.5–1105.5	−0.5[b]	33,400 ± 780	37,300 ± 1,100

[a]Calibration performed using Calib 6.0 with ΔR = 400 ± 200 years.
[b]Measured on separate sample from same depth interval.
[c]Measured from aliquot of ^{14}C sample.
[d]Not calibrated; sample has diagenetic overgrowth.

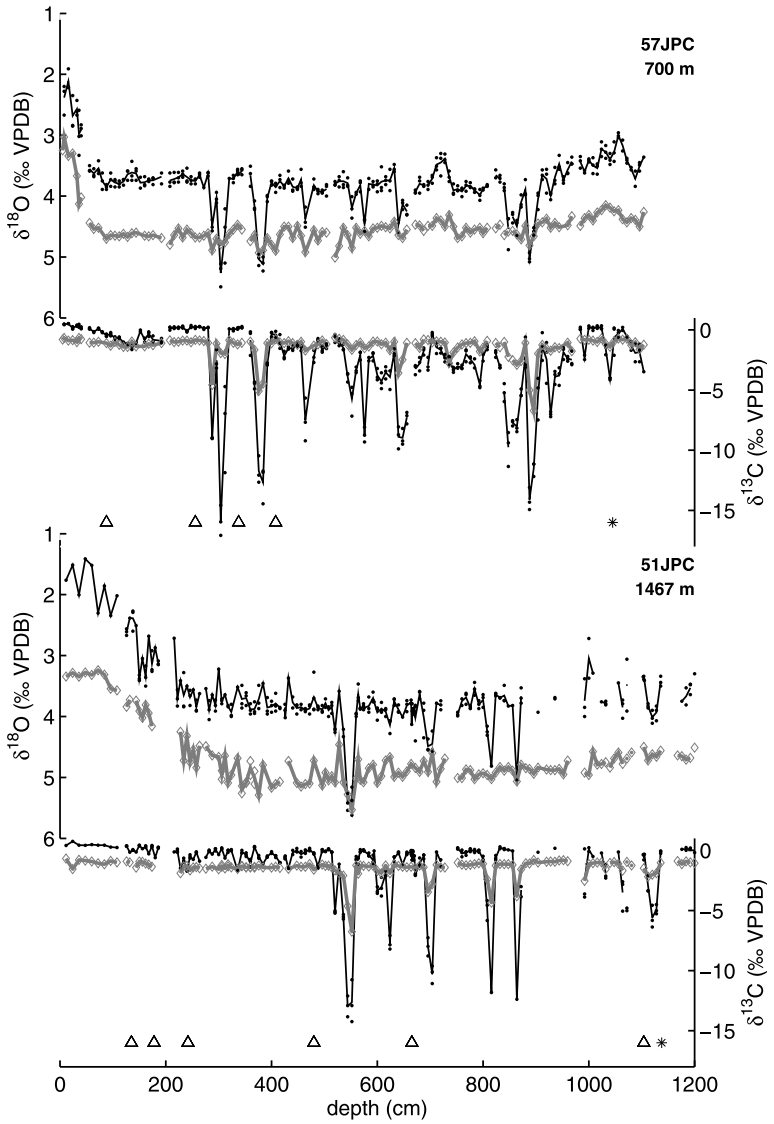

Figure 3. Stable isotope data from the planktic foraminifer *Neogloboquadrina pachyderma* (sinistral) in black and the benthic foraminifer *Uvigerina peregrina* in gray. Each symbol is a measurement of 8–10 *N. pachyderma* (s.) or one *U. peregina*. The lines connect mean values for each depth. The gaps are either core breaks or samples in which measurements could not be made. The triangles are the location of radiocarbon measurements on *N. pachyderma* (s.). The asterisk is a tie point between the two cores based on the magnetic susceptibility data (not shown).

[14] We made compound-specific $\delta^{13}C$ measurements on a Hewlett Packard 5890 gas chromatograph coupled to a Finnigan MAT 252 MS via a Thermo Electron GCC-II combustion interface. The GC column and temperature program were as described above. We corrected all $\delta^{13}C$ values of alcohols for the addition of carbon during derivatization using the measured $\delta^{13}C$ of the N,O-bis(trimethylsilyl)trifluoroacetamide reagent of −35.9‰.

3. Results

3.1. Foraminifer $\delta^{18}O$ and $\delta^{13}C$

[15] From the isotope data and calibrated radiocarbon dates, the Last Glacial Maximum (LGM) (defined as the maximum benthic $\delta^{18}O$) is at 88 cm in 57JPC and 376 cm in 51JPC (Figure 3). The sediment accumulation rate is lower in 57JPC during the deglaciation and Holocene, but the rates are nearly identical in the two cores during the late glacial period (46 cm kyr^{-1}, 18–25 kyr BP). The gaps in the isotope data in Figure 3 are the result of void spaces at the top of core sections due to settling after collection, or samples that did not contain enough foraminifera for analysis.

[16] During the glacial period, we find negative excursions in $\delta^{13}C$ of both *N. pachyderma* (s.) (as low as −17‰) and *U. peregrina* (as low as −6.8‰). The $\delta^{13}C$ excursions of *N. pachyderma* (s.) lower than −2‰ are marked with vertical gray bars in Figures 6, 7, and 9. In both cores, the anomalously low $\delta^{13}C$ is associated with high $\delta^{18}O$, as high

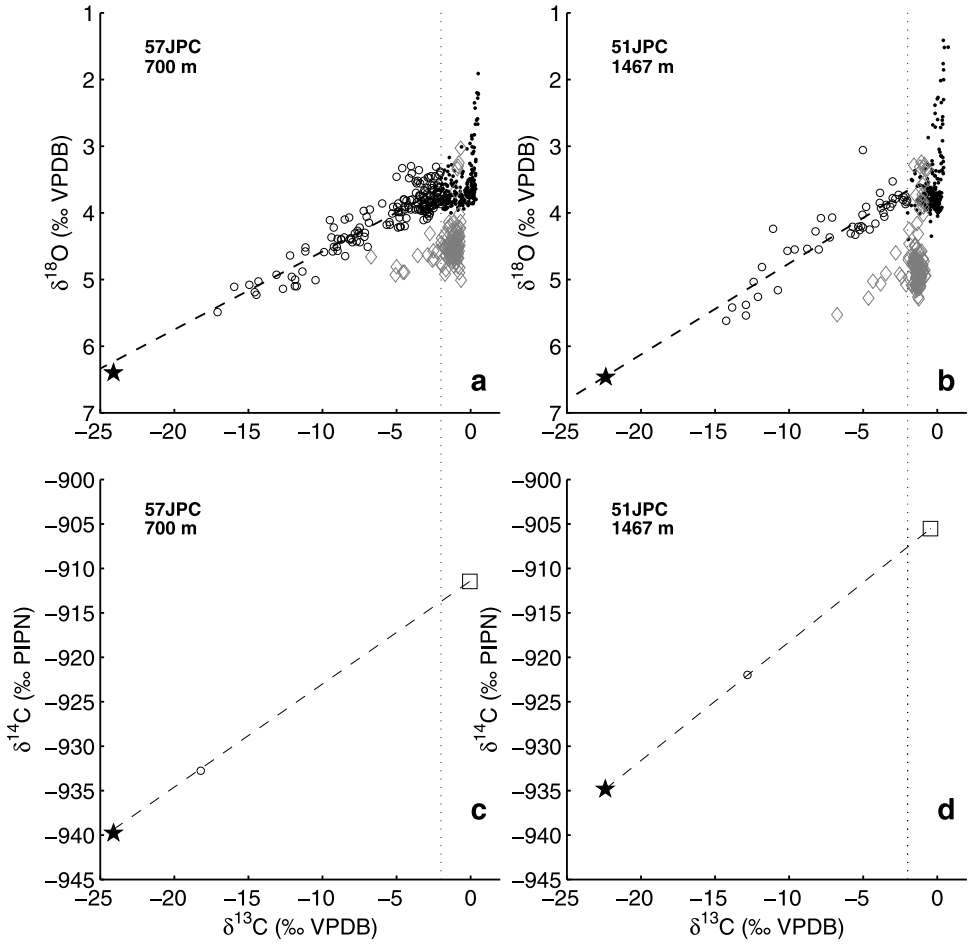

Figure 4. Stable isotope data. (a and b) Open circles and dots are *N. pachyderma* (s.), and diamonds are *U. peregrina*. The dotted line is drawn at $\delta^{13}C = -2‰$. Planktic measurements with $\delta^{13}C$ less than −2‰ are drawn with circles, and the linear least squares best fit line to those points is drawn with a dashed line. The star marks the estimate of the isotope composition of the authigenic end-member as calculated in Table 2. (c and d) The estimate of the $\delta^{14}C$ of the authigenic end-member as calculated in Table 3. The squares are the $\delta^{13}C$ and $\delta^{14}C$ of mean glacial *N. pachyderma* (s.). The circles are the $\delta^{13}C$ and $\delta^{14}C$ measured on *N. pachyderma* (s.) samples.

as 5.6‰. We plotted $\delta^{13}C$ versus $\delta^{18}O$ in Figures 4a and 4b. The planktic and benthic data with $\delta^{13}C$ less than −2‰ fall in clouds with trends toward decreasing $\delta^{13}C$ and increasing $\delta^{18}O$. Linear least squares lines fit through the *N. pachyderma* (s.) data with $\delta^{13}C$ less than −2‰ for 57JPC is

$$\delta^{18}O = -0.117\delta^{13}C + 3.41\left(n = 166; r^2 = 0.810; p < 10^{-60}\right).$$

For 51JPC, the best fit line is

$$\delta^{18}O = -0.137\delta^{13}C + 3.39\left(n = 47; r^2 = 0.805; p < 10^{-16}\right).$$

Photographs of samples with anomalous $\delta^{13}C$ and $\delta^{18}O$ show infilling of pores on the surface of *N. pachyderma* (s.) and between the costae of *U. peregrina* by a coarse-grained layer of yellowish minerals (Figure 5). We can apply a linear mass-mixing model to the data, where each sample with anomalously low $\delta^{13}C$ is composed of two end-members, foraminifer calcite and authigenic carbonate minerals. Depending on the fraction of the mass of the sample that is composed of foraminifer calcite (ϕ), the data fall along a mixing line between the compositions of the two end-members:

$$\delta^{18}O_{meas} = \delta^{18}O_{foram}\phi + \delta^{18}O_{auth}(1-\phi)$$

$$\delta^{13}C_{meas} = \delta^{13}C_{foram}\phi + \delta^{13}C_{auth}(1-\phi)$$

The linear best fit lines we calculated for the isotopically anomalous data are estimates of the mixing lines.

[17] To estimate the isotopic composition of the authigenic end-member, we compared two samples of *N. pachyderma* (s.) from a constrained size fraction (212–250 μm): one without overgrowth and one with overgrowth (Table 2). We assume that the individual foraminifera contain the same mass of foraminifer calcite, and the mass difference between samples with and without overgrowth is due to the addition of authigenic minerals. The measurements made of samples with overgrowth are $\delta^{13}C_{meas}$ and $\delta^{18}O_{meas}$. We assume that the $\delta^{13}C$ and $\delta^{18}O$ of the sample without overgrowth are the same as that of the foraminifer calcite of the sample

Figure 5. Photographs of foraminifera from HLY02-02-51JPC. (a) *N. pachyderma* (s.) (212–250 μm size fraction) and (c) *U. peregrina* (>250 μm size fraction) from 720 cm (without overgrowth). (b) *N. pachyderma* (s.) and (d) *U. peregrina* from 816 cm (with overgrowth). The width of the field of view in each panel is approximately 500 μm.

with overgrowth ($\delta^{13}C_{foram}$, $\delta^{18}O_{foram}$). There are appreciable uncertainties in this simplistic model, however, after substitution of these terms into the mixing equations the estimates of the isotopic composition of the authigenic carbonates are similar in the two cores. The $\delta^{13}C_{auth}$ and $\delta^{18}O_{auth}$ of the authigenic end-member in 57JPC are −24.1‰ and 6.4‰, respectively; in 51JPC, the $\delta^{13}C_{auth}$ and $\delta^{18}O_{auth}$ of the authigenic end-member are −22.4‰ and 6.5‰, respectively. These estimates are plotted as stars in Figures 4a and 4b and are consistent with our estimate of the mixing line.

Table 2. Estimate of Authigenic Carbonate $\delta^{13}C$ and $\delta^{18}O$

	ϕ	$\phi + a$	a
	HLY02-02-57JPC		
Depth (cm)	343.5–344.5	383.5–384.5	
Mass (μg)	4.7[a]	10.1[a]	5.4[b]
Fraction[b]	0.47	1.0	0.53
$\delta^{13}C$ (‰)	0.2[a]	−12.7[a]	−24.1[c]
$\delta^{18}O$ (‰)	3.6[a]	5.1[a]	6.4[c]
	HLY02-02-51JPC		
Depth (cm)	1103.5–1104.5	863.5–864.5	
Mass (μg)	2.4[a]	5.3[a]	2.9[b]
Fraction[b]	0.46	1.0	0.54
$\delta^{13}C$ (‰)	−0.6[a]	−12.4[a]	−22.4[c]
$\delta^{18}O$ (‰)	3.4[a]	5.0[a]	6.5[c]

[a]Measured.
[b]We assume that the mass difference between *N. pachyderma* (s.) (212–250 μm size fraction) with ($\phi + a$) and without (ϕ) authigenic overgrowth is entirely due to the addition of authigenic carbonate minerals (a).
[c]Calculated from a linear mixing model where $\delta_m = \delta_f \phi + \delta_a(1 - \phi)$.

3.2. Foraminifer $\Delta^{14}C$

[18] The results of the ^{14}C measurements of *N. pachyderma* (s.) and calibration to calendar ages are in Table 1. The ^{14}C measurements used for the age model were on samples of *N. pachyderma* (s.) that had $\delta^{13}C$ greater than −2‰ and therefore had little or no authigenic minerals. The isotopic record spans the late glacial period (~40 cal kyr BP) to the Holocene. According to the linear age models, the three stratigraphically highest isotopic events in the two cores are contemporaneous, occurring at 22, 24, and 26 ka (Figure 6).

[19] In addition to the ^{14}C measurements for the age model, in each core, we made ^{14}C measurements of *N. pachyderma* (s.) from a sample within an excursion (Table 3). The conventional radiocarbon ages of these samples are older than expected from the adjacent radiocarbon measurements, which is consistent with the samples being a mixture of ^{14}C-depleted authigenic carbonates and foraminifer calcite. In Table 3, we estimate the $\Delta^{14}C$ of the authigenic carbonate minerals. The first step was to estimate the $\Delta^{14}C$ of the foraminifer calcite in the sample with authigenic overgrowth using the Marine09 [*Reimer et al.*, 2009] during the interpolated calendar age of the sample, assuming ΔR of 400 ± 200 years. Using the true decay constant of radiocarbon (λ = 8267^{-1} years^{-1}) [*Godwin*, 1962], we "aged" the samples by their calendar age to estimate what the foraminifer calcite $\Delta^{14}C$ would be in modern times (1950 CE). The next step was to estimate the fraction of the samples composed of foraminifer calcite using the same linear mixing model as in Table 2, and calculate the fraction of the samples (ϕ) that is foraminifer calcite. Before applying the linear mixing

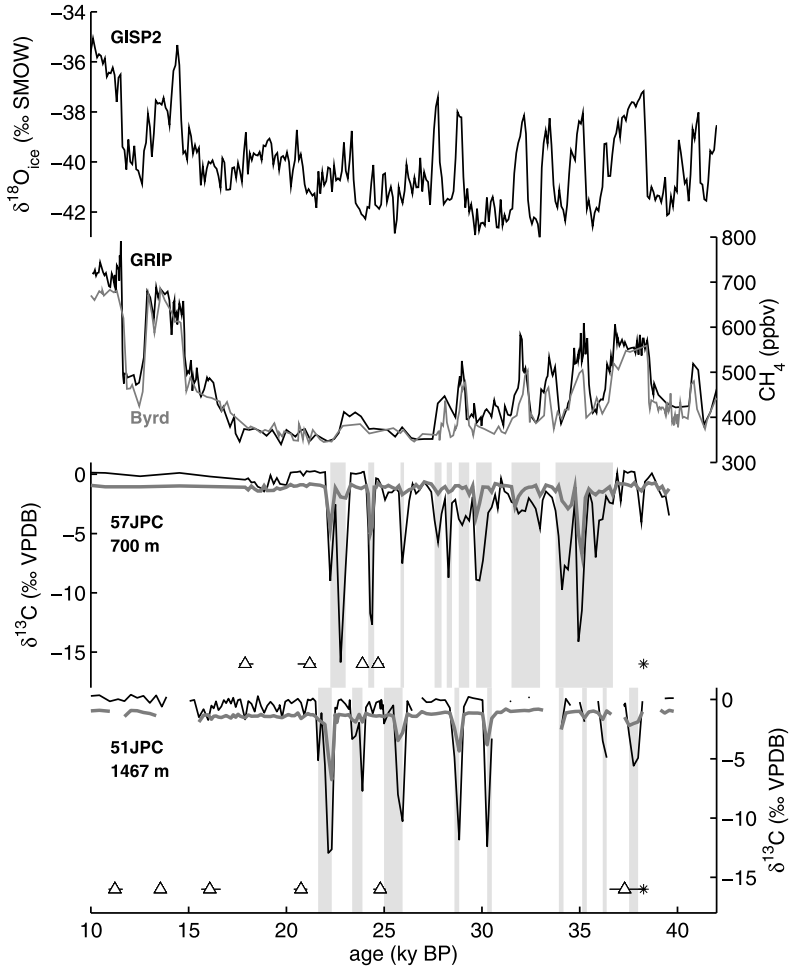

Figure 6. (bottom) The *N. pachyderma* (s.) (black) and *U. peregrina* (gray) $\delta^{13}C$ data from HLY02-02-57JPC and 51JPC plotted against calendar age. Black triangles mark depths of calibrated *N. pachyderma* (s.) foraminifer radiocarbon ages, with the horizontal line showing the 1σ uncertainty. The asterisk is the tie point between the two cores based on magnetic susceptibility. Horizontal gray bars mark samples in which the $\delta^{13}C$ of *N. pachyderma* is less than −2‰. (top) The $\delta^{18}O_{ice}$ from the GISP2 ice core on the ss09sea age model [*Johnsen et al.*, 2001] and the concentration of atmospheric methane measured in the GRIP (black) and Byrd (gray) ice cores [*Blunier and Brook*, 2001].

model to the ^{14}C data, we removed the correction for biological fraction. Next we used the linear mixing equation with $\delta^{14}C$, $\delta^{14}C_f$, and ϕ to calculate $\delta^{14}C_a$, the $\delta^{14}C$ of the authigenic carbonate minerals, and then reapplied the correction for biological fractionation. Since the $\Delta^{14}C$ of atmospheric CO_2 was higher during MIS3 than today, to make a comparison to the modern ocean system, we applied the decay equation to correct the $\Delta^{14}C_a$ to a world where the mean $\Delta^{14}C$ of the atmosphere is 0‰ and the surface ocean with the local reservoir correction ($R + \Delta R$ = 400 + 400 years) is −92‰. These corrected values, $\Delta^{14}C_a$*, are −350‰ in 57JPC and −345‰ in 51JPC.

3.3. Benthic Foraminifer Abundance

[20] We counted the abundance of benthic foraminifer species through three isotope excursions in 57JPC (256–496 cm) and five in 51JPC (496–904 cm). The six most common benthic foraminifer species are *Buliminella* sp., *Elphidium* cf. *batialis*, *Globobulimina pacifica*, *Islandiella norcrossi*, *Nonionella labradorica* and *U. peregrina*. In 57JPC, *U. peregrina* and *N. labradorica* are the dominant species present, while in 51JPC, *N. labradorica* is dominant.

[21] The absolute abundance of benthic foraminifera is significantly correlated with *N. pachyderma* (s.) $\delta^{13}C$ in both 57JPC and 51JPC ($r = -0.41$, $r^2 = 0.17$, $p = 0.03$; $r = -0.37$, $r^2 = 0.14$, $p = 0.01$), where there is a higher abundance of benthic foraminifera during episodes of low $\delta^{13}C$ (Table 4 and Figure 7). In 57JPC, the highest benthic abundances were measured during the isotope excursion at 312 cm (165 g^{-1}). In 51JPC, the highest benthic abundances were measured during isotope excursions at 520 cm (301 g^{-1}) and 624 cm (102 g^{-1}). The coefficients of determination are relatively low, indicating that benthic foraminifer abundance is influenced by factors other than those associated with the isotopic anomalies (Table 4).

[22] In 57JPC, *N. labradorica* and *G. pacifica* abundances are significantly correlated with *N. pachyderma* (s.) $\delta^{13}C$ and are relatively high during each of the 3 isotope excursions,

Table 3. Estimate of the $\Delta^{14}C$ of Authigenic Carbonate ($\Delta^{14}C_a$)

	HLY02-02-57JPC, 303.5–304.5 cm	HLY02-02-51JPC, 543.5–544.5 cm
^{14}C age[a] (years)	21,800	20,700
calendar age[b] (years BP)	22,770	22,150
$\delta^{13}C_m$[a] (‰)	−18.2	−12.8
$\Delta^{14}C_m$[a] (‰)	−933.7	−923.9
$\delta^{14}C_m$[c] (‰)	−932.8	−922.0
N. pachyderma (s.) Test		
$\delta^{13}C_f$[d] (‰)	0.0	−0.5
$\Delta^{14}C_f$[e] (‰)	−916	−910
$\delta^{14}C_f$[c] (‰)	−911	−906
ϕ[f]	0.24	0.44
Authigenic Carbonate		
$\delta^{13}C_a$[g] (‰)	−24.1	−22.4
$\delta^{14}C_a$[c,h] (‰)	−940	−935
$\Delta^{14}C_a$ (‰)	−940	−935
$\Delta^{14}C_a$*[i] (‰)	−350	−345

[a]Measured.
[b]Linearly interpolated from adjacent calibrated dates.
[c]Without correction for biological fractionation, $\Delta^{14}C = 1000\left[\left(\frac{\delta^{14}C}{1000}+1\right)\left(\frac{1-0.025}{1+\delta^{13}C/1000}\right)^2-1\right]$.
[d]Mean $\delta^{13}C$ of *N. pachyderma* (s.) 20–25 kyr BP, where $\delta^{13}C > -2$‰.
[e]Marine09 $\Delta^{14}C$ during the interpolated calendar age of sample, with $\Delta R = 400 \pm 200$ years, "aged" using the true decay constant ($\lambda = 8267^{-1}$ years^{-1}) to 1950.
[f]Fraction of sample that is *N. pachyderma* (s.) test, with $\delta^{13}C_a$ from Table 2, $\delta^{13}C_f$ calculated in this table, measured $\delta^{13}C_m$, and where $\phi = \frac{\delta_m-\delta_a}{\delta_f-\delta_a}$.
[g]The $\delta^{13}C$ of authigenic carbonate (from Table 2).
[h]Where $\delta_a = \frac{\delta_m-\delta_f\phi}{1-\phi}$.
[i]Corrected for a world with a mean atmospheric $\Delta^{14}C$ of 0‰ and $\Delta^{14}C_f$ of −92‰ ($R + \Delta R = 800$ years) for comparability with modern seep systems.

while during the shallowest isotope excursion, *E.* cf. *batialis* peaks at 24 g^{-1} at 312 cm, which is around five times higher than the local maxima during the other two isotope excursions (Figure 7). In 51JPC, the dominant species, *N. labradorica*, mirrors the maximum abundances of total benthic foraminifera during the isotope excursions at 520 cm (281 g^{-1}) and 624 cm (79 g^{-1}). There are maxima in *G. pacifica* during each of the 5 isotope excursions. For all the species with significant correlation to *N. pachyderma* (s.) $\delta^{13}C$, the coefficients of determination are relatively low (Table 4), and there is variability in the abundances that is not related to the isotopic excursions.

3.4. Biomarkers

[23] The dominant compounds in all samples included *n*-alcohols (with 22 to 28 carbons) with $\delta^{13}C$ varying from −35 to −30‰, and isololiolide and loliolide with $\delta^{13}C$ of −25 to −22‰ (Figure 8). The abundance of bacterial and archaeal lipids varied and was generally greater in samples within or just below the horizons with low foraminiferal $\delta^{13}C$ (Figure 9).

[24] The dominant archaeal lipid identified was archaeol (Figure 9; structure a in Figure S2 in the auxiliary material).[1] The $\delta^{13}C$ of archaeol was measureable in only five samples in 51JPC, with values between −79‰ and −72‰ (Figure 9). These samples were within or just below horizons of low *N. pachyderma* (s.) $\delta^{13}C$. In 57JPC, the concentration of archaeol was too low to measure its $\delta^{13}C$ in any samples.

[25] The most abundant bacterial lipid was di-*anteiso*-C_{15}-glyceroldiether (DAGE-C_{30}) (Figure 9; structure b in Figure S2). Changes in concentration of this compound were similar to the changes observed in archaeol, which is more abundant in samples within or just below horizons of low *N. pachyderma* (s.) $\delta^{13}C$ (Figure 9). In 51JPC, the $\delta^{13}C$ of the DAGE-C_{30} decreased from an average value of −42‰ in 493.5–418 cm to a minimum value of −60‰ at 557 cm. In 57JPC, the decrease in $\delta^{13}C$ is smaller, from an average of −47‰ in 262–286 cm to a minimum value of −51‰ at 310 cm.

[26] In 51JPC, the $\delta^{13}C$ of all biphytanes from ether-cleaved GDGTs (structures c–f in Figure S2) at 504.5 and 518 cm are similar, with an average value of −22‰ (σ = 1‰) (Figure 9). At 557 cm, just below the minimum *N. pachyderma* (s.) $\delta^{13}C$, the $\delta^{13}C$ of acyclic and monocyclic biphytane decreases to minimum values of −28‰ and −58‰, respectively. In 57JPC, the mean $\delta^{13}C$ of all biphytanes at 278 and 286 cm is −22‰ (σ = 1‰). At 310 cm, the $\delta^{13}C$ of monocyclic and acyclic biphytane decrease to minimum values of −29‰ and −26‰, respectively. The $\delta^{13}C$ of bicyclic and tricyclic biphytane do not change significantly in either core. The yield from ether cleavage reactions is typically low and variable, and we did not use an alcohol recovery standard to quantify yield. Consequently, we did not make estimates of the concentration of the cleaved compounds.

4. Discussion

4.1. Evidence of Periodically Enhanced Methane Flux

[27] The anomalously low $\delta^{13}C$ and $\Delta^{14}C$ measured in the planktic and benthic foraminifer samples are the result of mixing between foraminifer calcite and authigenic carbonates associated with anaerobic oxidation of methane (AOM). This two-end-member mixing has been observed in foraminifera from modern active seeps, including at Hydrate Ridge [*Orphan et al.*, 2004] and Papua New Guinea [*Schmidt et al.*, 2002]. Not all foraminifera with low $\delta^{13}C$ have authigenic overgrowths as obvious as the examples in Figure 5. A small amount of authigenic carbonate on or within the test could account for the isotopic anomalies.

Table 4. Regression Between Benthic Foraminifera Abundance and *N. pachyderma* (s.) $\delta^{13}C$[a]

	HLY02-02-57JPC			HLY02-02-51JPC		
	r	r^2	p	r	r^2	p
Total benthic foraminifera	**−0.41**	**0.17**	**0.03**	**−0.37**	**0.14**	**0.01**
Nonionella labradorica	**−0.56**	**0.32**	**0.002**	**−0.37**	**0.14**	**0.01**
Globulimina pacifica	**−0.36**	**0.13**	**0.06**	**−0.46**	**0.21**	**0.001**
Elphidium cf. *batialis*	**−0.40**	**0.16**	**0.03**	0.03	0.00	0.9
Buliminella sp.	0.11	0.01	0.6	**−0.28**	**0.08**	**0.06**
Uvigerina peregrina	−0.13	0.02	0.5	−0.10	0.01	0.5
Islandiella norcrossi	0.14	0.02	0.5	0.22	0.05	0.1

[a]Boldface denotes correlation that is statistically significant with at least 94% certainty.

[1]Auxiliary materials are available in the HTML. doi:10.1029/2010PA001993.

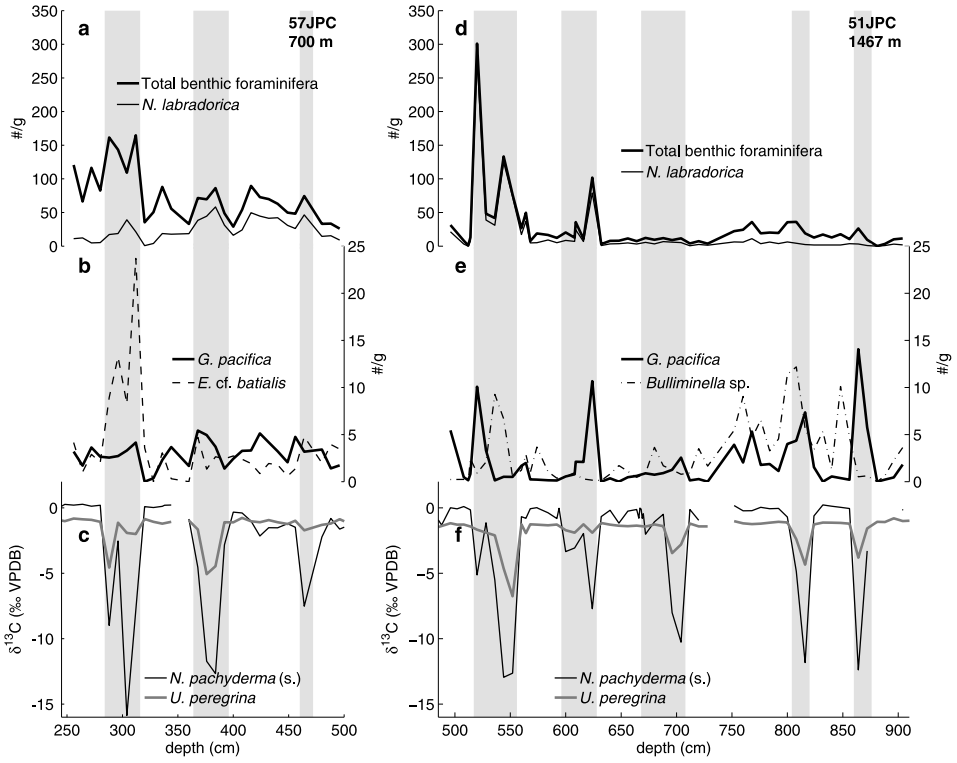

Figure 7. Absolute abundance of benthic foraminifera per gram dry sediment. In HLY02-02-57JPC, (a) total benthic foraminifera (thick line) and *N. labradorica* (thin line) and (b) *G. pacifica* (thick line) and *E.* cf. *batialis* (dashed line). (c) The δ^{13}C of *N. pachyderma* (s.) (black) and *U. peregrina* (gray). The vertical gray bars mark samples in which the *N. pachyderma* (s.) δ^{13}C is less than −2‰. In 51JPC, (d) total benthic foraminifera (thick line) and *N. labradorica* (thin line) and (e) *G. pacifica* (thick line) and *Buliminella* sp. (dotted line). (f) The δ^{13}C of *N. pachyderma* (s.) (black) and *U. peregrina* (gray). The vertical gray bars mark samples in which the *N. pachyderma* (s.) δ^{13}C is less than −2‰.

Based on the average δ^{13}C of *N. pachyderma* (s.) during the glacial period, the estimated δ^{13}C of the authigenic carbonates, and the mass mixing model, samples that have δ^{13}C less than −2‰ are at least 8% authigenic carbonate by mass. The isotopic anomalies are larger for *N. pachyderma* (s.) than *U. peregrina* (Figure 3), probably due to the high surface area of a planktic foraminifer test, which is more likely to accommodate contamination by small crystals of authigenic carbonate than the imperforate test of *U. peregrina*.

[28] Since the two-end-member mixing model is also consistent with the stable isotope composition of *U. peregrina*, this means that the calcite test has an isotopic composition distinct from the authigenic carbonate minerals, and that the foraminifera must have calcified its test before the authigenic minerals precipitated. This is similar to observations at Hydrate Ridge [*Torres et al.*, 2003], where Rose Bengal–stained benthic foraminifera had δ^{13}C much higher than the pore waters in which they were collected, implying that the benthic foraminifera calcified their tests during periods of lower methane flux, or grew before active methane oxidation began. In contrast at southern Hydrate Ridge [*Hill et al.*, 2004], individual Rose Bengal–stained benthic foraminifera had variable δ^{13}C, with values as low as −12.6‰, and whose shells, studied with scanning electron microscopy, had no visible evidence of diagenesis or authigenic carbonates, implying the calcite in the foraminifer tests incorporated methane-derived carbon. It is possible that there is some variability in the δ^{13}C of the *U. peregrina* tests that we studied, which would change the foraminifer calcite end-member δ^{13}C. The current data are insufficient to test for this possibility, and many of our samples clearly have authigenic carbonates.

[29] The δ^{18}O we estimate for the authigenic carbonate is 1.5–1.6‰ higher than mean δ^{18}O of *U. peregrina* measured between low δ^{13}C events in samples 20–25 ka. This enrichment in ^{18}O is not likely to be caused by a decrease in the bottom water temperature, since today, the temperatures at the two coring sites are 2.2°C at 51JPC and 3.2°C at 57JPC, and a benthic δ^{18}O record from 2209 m at Bowers Ridge exhibits no remarkable changes during MIS3 [*Brunelle et al.*, 2007]. It is also unlikely to be due to water from dissociated methane hydrates, which is ~3‰ enriched in ^{18}O [*Matsumoto and Borowski*, 2000], since it would require pore water to be 50% hydrate water. This site is deep enough that even large changes in temperature are unlikely to cause significant destabilization of methane hydrates [*Xu and Lowell*, 2001].

[30] The mineralogy of the authigenic minerals is probably the main influence on their δ^{18}O. In modern cold seeps, the authigenic carbonates can be composed of high-Mg (magnesian) calcite, aragonite and/or dolomite [*Peckmann and Thiel*, 2004]. The fractionation of oxygen isotopes as a function of temperature was determined experimentally by

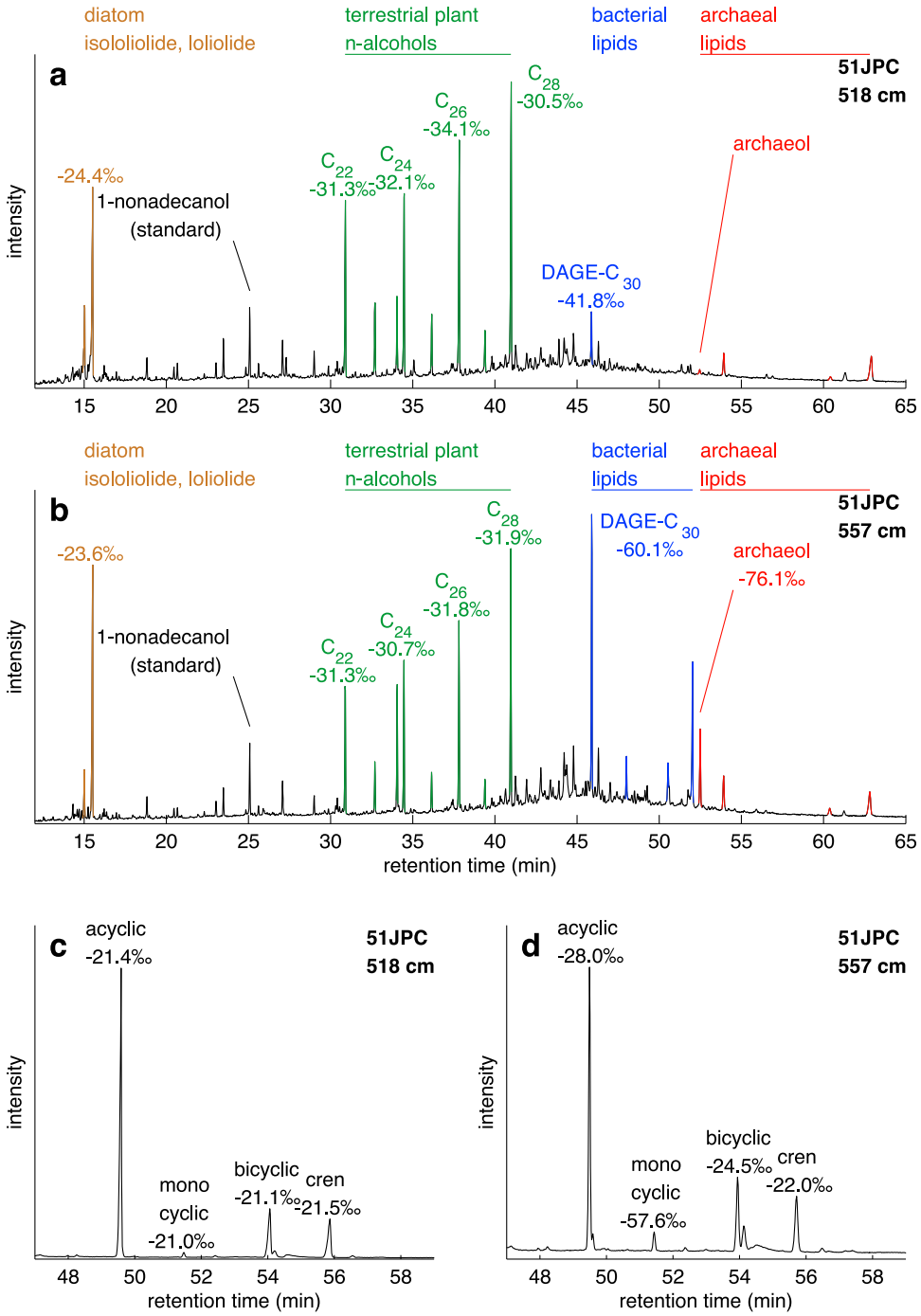

Figure 8. Total ion current chromatograms from HLY02-02-51JPC (a and c) 518 cm and (b and d) 557 cm. Figures 8a and 8b are the alcohols, analyzed as their TMS derivatives. Provenance of major compounds is labeled, as well as their $\delta^{13}C$ as measured with GC-IRMS. Figure 8c and 8d are excerpts from the chromatograms of the tetraether-derived biphytanes from these samples, showing their $\delta^{13}C$ values as measured with GC-IRMS. Cren is tricyclic biphytane, containing two pentacyclic, one hexacyclic ring. DAGE-C_{30} is di-*anteiso*-C_{15}-glyceroldiether.

Kim and O'Neil [1997] for calcite (at 10–40°C), by *Kim et al.* [2004] for aragonite (at 5–40°C), and by *Fritz and Smith* [1970] for dolomite (at 25–79°C). At low temperatures, the $\delta^{18}O$ of aragonite and calcite are very similar, but dolomite $\delta^{18}O$ is on average 2.6‰ higher. In magnesian calcite there is greater incorporation of ^{18}O with higher molar fraction of Mg in the mineral [*Tarutani et al.*, 1969]. The $\delta^{18}O$ and Mg/Ca (see auxiliary material) of the authigenic minerals is consistent with the presence of dolomite and/or magnesian calcite.

[31] The $\delta^{13}C$ of DIC of pore water influenced by AOM is strongly dependent on methane flux which will ultimately

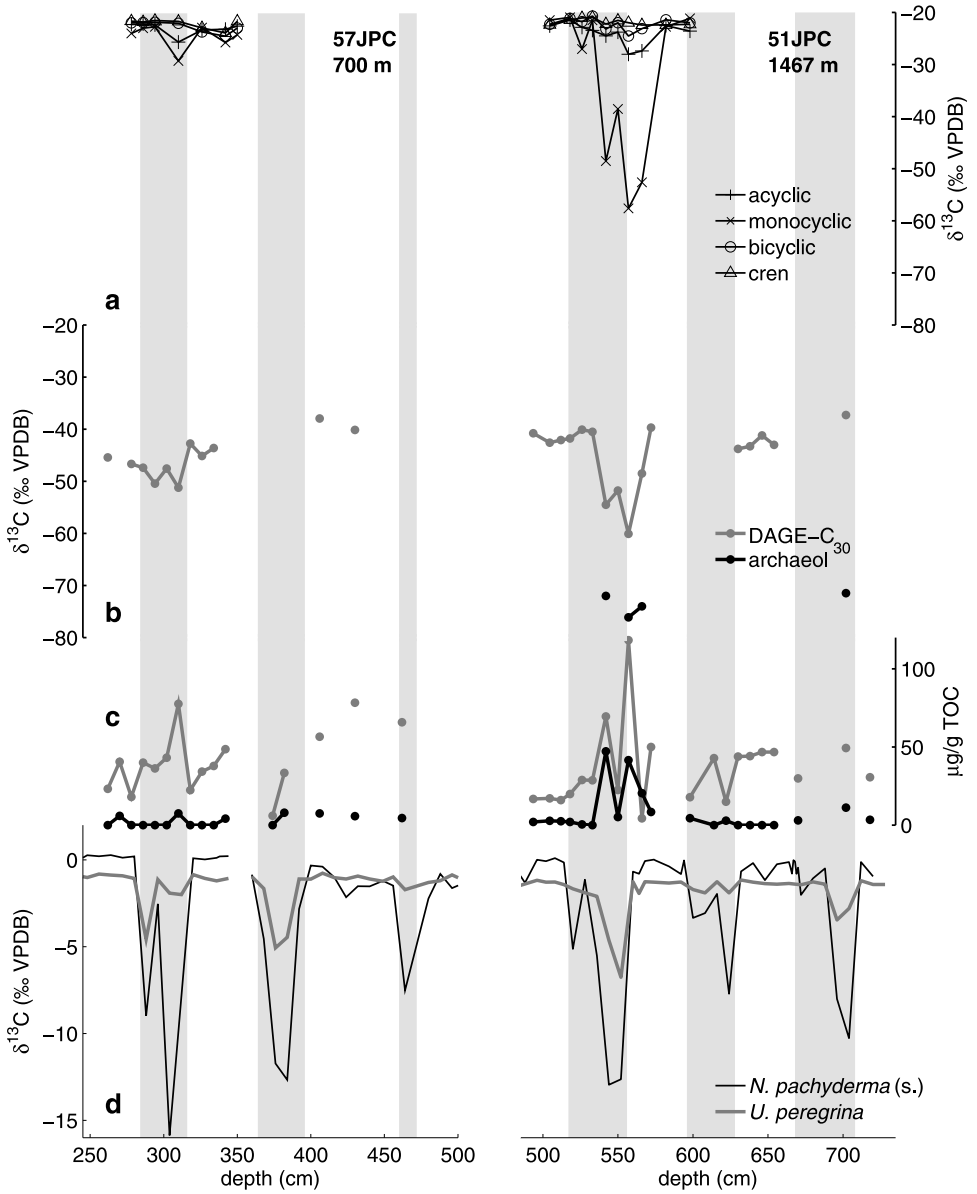

Figure 9. Biomarker data from (left) HLY02-02-57JPC and (right) 51JPC. (a) The δ^{13}C of hydrocarbons derived from ether cleavage and subsequent reduction of ether lipids. Acyclic, monocyclic, bicyclic and tricyclic (cren) biphytanes are constituents of GDGT core lipids. (b) The δ^{13}C of archaeol and di-*anteiso*-C_{15}-glyceroldiether. (DAGE-C_{30}). (c) The concentration of archaeol and DAGE-C_{30}. (d) *N. pachyderma* (s.) (black) and *U. peregrina* (gray) δ^{13}C data, and gray vertical bars mark samples in which the planktic δ^{13}C is less than −2‰. Cren is tricyclic biphytane, containing two pentacyclic, one hexacyclic ring.

determine methane oxidation rate and the depth of the SMTZ [*Borowski et al.*, 1996]. Our estimates of the δ^{13}C of the authigenic carbonates (−24.1 and −22.4‰ in 57JPC and 51JPC, respectively) could be consistent with high AOM rates and a very shallow SMTZ or more moderate AOM rates and deeper SMTZ [*Zeebe*, 2007]. For example, they are similar to the δ^{13}C of carbonate crusts from mud volcanoes from the eastern Mediterranean (−28.9‰ and −24.8‰ at the sediment-water interface [*Aloisi et al.*, 2002]), and in sediments from the Chilean Margin (−24.6‰ at 355 cm below seafloor [*Treude et al.*, 2005]).

[32] The DIC that originates from fossil methane deep within the sediment column is radiocarbon free [*Winckler et al.*, 2002], and with high methane flux toward the seafloor, could incorporate carbon from younger carbon reservoirs [*Kessler et al.*, 2008]. Samples of *N. pachyderma* (s.) with authigenic carbonates appear 2000–3000 years older than would be expected from the age model (Table 1), similar to observations of authigenic carbonates from the Japan margin [*Uchida et al.*, 2008]. The lower Δ^{14}C in the authigenic carbonates is equivalent to −350‰ and −345‰ in the present day. This is not as low as radiocarbon measurements on authigenic carbonates at modern seeps in the

Gulf of Mexico (−898‰ to −992‰ [*Aharon et al.*, 1997]), Aleutian accretionary margin (−860‰ [*Greinert et al.*, 2002]) or the Black Sea (−918‰ to −901‰ BP [*Peckmann et al.*, 2001]). However, the $\delta^{13}C$ of the carbonates at these sites were lower than in this study, implying that they had a higher proportion of methane-derived DIC, and would be expected to have a carbon pool more depleted in ^{14}C as well.

[33] Deviation of the isotope measurements from the theoretical mixing lines (Figure 4) could be the result of variations in the isotopic composition of the foraminifer and authigenic carbonate end-members from event to event. However, since we can use a single mixing model to describe the *N. pachyderma* (s.) and *U. peregrina* $\delta^{18}O$, $\delta^{13}C$ and $\Delta^{14}C$ in each core, the isotopic composition of DIC during the recurring episodes of authigenic carbonate precipitation were similar, even given the simplified mixing model. This suggests that the multiple events through time and in the two study regions may have drawn from the same carbon pool, and that these episodes were not strictly local, transient phenomena.

[34] Lipid biomarkers can give clues as to the intensity and location of AOM. Assuming that the $\delta^{13}C_{methane}$ here is similar to that observed by *Claypool et al.* [1973] (mean = −72‰, σ = 4‰, n = 13), $\delta^{13}C_{archaeol}$ is up to 4‰ lower than $\delta^{13}C_{methane}$ (Figure 9). At settings with intense AOM, $\delta^{13}C$ values of archaeaol are typically lower than those of methane (by up to −50‰) [e.g., *Peckmann and Thiel*, 2004]. The most plausible interpretation is that the values observed here represent a mixed origin of archaeol of methanogenic and methanotrophic archaea. Production of these respective fractions likely did not occur simultaneously. Rather, we suggest that the methanotrophic portion formed during a punctuated event when conditions where conducive of AOM, while methanogenic production of archaeol extended over longer periods after burial in the subsurface. This interpretation is consistent with the concentration profile that suggests methanogenic background production of archaeol throughout most of the sediment column, and concentration maxima that coincide with increased ^{13}C depletion. A similar mixed origin was inferred in a late Quaternary record from the Santa Barbara Basin (SBB), where only during an event at around 44 ka, $\delta^{13}C_{archaeol}$ showed a negative spike of −25‰ lower than background values [*Hinrichs et al.*, 2003]. Minimum $\delta^{13}C$ values of archaeol in SBB coincided with the sudden appearance of several ^{13}C-depleted dialkylglycerolethers (DAGEs), which are likely derived from sulfate reducing bacteria [e.g., *Hinrichs et al.*, 2000], as well as minima in the $\delta^{13}C$ of both benthic and planktic foraminifera [*Hinrichs et al.*, 2003; *Kennett et al.*, 2000].

[35] Additional information on anaerobic methanotrophic communities in our study area is from analysis of GDGT-derived biphytanes. Methane oxidizing archaea of the ANME-1 cluster are known to produce substantial amounts of GDGTs with zero to three cyclopentanes [e.g., *Rossel et al.*, 2008; *Wakeham et al.*, 2003]. In marine sediments, several groups of metabolically distinct archaea need to be considered as sources of GDGTs: planktic crenarchaea, which can be preserved well in marine sediments [e.g., *Schouten et al.*, 1998; *Sinninghe Damasté et al.*, 2002]; benthic archaea, including methanogens [e.g., *Koga and Nakano*, 2008], methanotrophs [e.g., *Hinrichs et al.*, 2000]; and other heterotrophic archaea [e.g., *Biddle et al.*, 2006]. GDGT-0 (caldarchaeol, no rings) is a common constituent in polar lipids of a wide range of methanogens, GDGT-1 and -2 (one and two cyclopentane rings) are rare among cultured methanogens [e.g., *Koga and Nakano*, 2008]. Both planktic and benthic archaea produce primarily GDGT-0 (caldarchaeol) and GDGT-5 (crenarchaeol, four cyclopentane rings and one cyclohexane ring) and smaller amounts of GDGT-1 and -2, with typical $\delta^{13}C$ values for the constituent biphytanes ranging from −30‰ to −20‰ [*Biddle et al.*, 2006; *Hoefs et al.*, 1997].

[36] The relative distribution of GDGT-cleaved biphytanes in all our samples reflects strong contribution of crenarchaea, with the greatest abundance of acyclic biphytane (predominantly GDGT-0 derived) and similar abundances of bicyclic and tricyclic biphytane (predominantly GDGT-5 derived), and small amounts of monocyclic biphytane (derived from GDGT-1 and -2) (Figure 8). The $\delta^{13}C$ values of bicyclic and tricyclic biphytanes fall within the typical range observed in planktic and benthic archaea. The low $\delta^{13}C$ values of monocyclic biphytane in both sediment cores indicate the contribution of GDGT-1 and -2 from methanotrophic archaea. The maximum ^{13}C-depletion in this compound is consistent with the high relative abundance of GDGT-1 and -2 in methanotrophic archaea. The lower degree of ^{13}C-depletion in acyclic biphytane is because the greatest proportion of this compound is most likely derived from planktic and unknown heterotrophic benthic archaea [cf. *Biddle et al.*, 2006; *Lipp and Hinrichs*, 2009; *Schouten et al.*, 2002].

[37] The ^{13}C-depleted bacterial lipids that cooccur with ^{13}C-depleted archaeol and GDGT-derived biphytanes (Figure 8) are likely from syntrophic sulfate reducing bacteria (SRB). DAGEs from SRBs are typical for sediments hosting ANME consortia [*Blumenberg et al.*, 2004; *Hinrichs et al.*, 2000; *Teske et al.*, 2002]. Background $\delta^{13}C$ values of DAGE-C_{30} are −47 to −42‰. In samples where ^{13}C-depleted archaeal lipids indicate the presence of methanotrophic biomass, the $\delta^{13}C$ of the DAGE-C_{30} drops, reflecting the contribution of a methane-derived substrate to the SRB.

[38] Notably, we did not detect diplopterol or diploptene in any samples, which would indicate aerobic, bacterial-driven methanotrophy within the water column [*Hinrichs*, 2001; *Summons et al.*, 1994]. Though the benthic foraminiferal abundances suggest release of methane into the water column, it is possible that any aerobic methanotrophic biomass was low enough to be undetectable, resulting in a lipid profile that represents exclusively the sedimentary anaerobic methanotrophic biomass.

[39] Even with methane release into the water column, a substantial flux of methane into the atmosphere would be required to trigger greenhouse warming. Bacterial methanotrophy in the oceanic water column is highly effective (see review by *Reeburgh* [2007]), and in the modern ocean, methane flux to the atmosphere from shallow submarine seeps and mud volcanoes is considered small [*Judd*, 2000], with virtually no methane from deeper sites reaching the atmosphere [*McGinnis et al.*, 2006]. However, with sudden, high methane flux, a rising bubble plume could advect a mixture of methane-saturated seawater and gas bubbles toward the surface, allowing methane flux from water depths greater than 250 m to reach the atmosphere [*Leifer et al.*,

2006]. Recent measurements from the Gulf of Mexico suggest that current estimates of methane bubble dissolution may be too low, and flux from deepwater seeps may be larger than previously assumed [*Solomon et al.*, 2009].

4.2. Location of AOM in Sediment Column

[40] Only the events associated with the strongest ^{13}C depletion in foraminifera are associated with unambiguous molecular signals indicative of AOM (304 cm in 57JPC, 544 cm in 51JPC). We suggest that only some of the authigenic carbonate layers were associated with rates of methane oxidation high enough and for long enough to emplace sufficient methanotrophic biomass for detection. The carbon conversion efficiency of methane into biomass for methanotrophs is quite low [*Wegener et al.*, 2008]. As a consequence, molecular signals of AOM communities remained elusive for decades, especially in settings where low diffusive flux is linked to relatively low rates of AOM [cf. *Bian et al.*, 2001]. In an example from the North Sea, *Niemann et al.* [2005] measured elevated sulfate reduction and methane oxidation rates in the SMTZ of an active methane seep, but no lipid biomarkers from the methane oxidizing microbial community were found.

[41] If the SMTZ is deep in the seafloor, the authigenic carbonates form in sediment that is much older than the episode of methane flux, and consequently all of the methane is oxidized within the sediment column [*Treude et al.*, 2005; *Ussler and Paull*, 2008]. If this is the case in our study region, the age of the sediments containing authigenic carbonates would not be the same as the time the methane flux occurred. Therefore, it is important to establish where in the sediment column the SMTZ was when the authigenic carbonates precipitated.

[42] Faunal change has been used to identify episodes of methane seepage in the past where relatively high abundance of endobenthic foraminifera and high absolute abundance of benthic foraminifera were interpreted as indicating methane seepage [*Bhaumik and Gupta*, 2007; *Wiedicke and Weiss*, 2006]. However, in the modern system, benthic foraminifer densities are highly variable within seeps [*Heinz et al.*, 2005; *Rathburn et al.*, 2000] and outside of seeps [*Bernstein et al.*, 1978]. There does not appear to be a unique assemblage of seep fauna or an endemic species of benthic foraminifera in seeps, but dominant species frequently include members of the genera *Uvigerina*, *Bolivina*, *Epistominella* and *Nonionella* (see references in the work by *Heinz et al.* [2005]).

[43] There is the added uncertainty that all of the surveys of the abundance and species of benthic foraminifera living in seep areas referenced above rely on Rose Bengal, a protein marking stain, to identify "living" specimens. However, Rose Bengal will stain tests that contain any cytoplasm, even if the individual is dead [*Bernhard*, 1988]. *Bernhard et al.* [2001] studied fauna in an active seep in Monterey Bay using a metabolic fluorescent tag that only labels adenosine triphosphate, which is only present in living cells, and observed that living individuals of *Epistominella*, *Fursenkoina*, and *Spiroplectammina* were more common in seep sediments than nonseep sediments. The seep assemblage also included *Uvigerina*, *Bulimina*, and *Cassidulina*, consistent with Rose Bengal–based studied at other seep sites.

[44] Though there is no diagnostic fauna present in modern seeps, a large geochemical change in the habitat of benthic foraminifera occurs with the initiation of a methane seep, and a change in the benthic fauna that is coincident with other geochemical tracers of high methane flux would suggest methane seeping from the seafloor. In both our study areas, absolute abundance of benthic foraminifera, *N. labradorica* and *E.* cf. *batialis* increases in several of the horizons with authigenic carbonates (Table 4 and Figure 7). In 51JPC, the absolute abundance of *G. pacifica* increases during each horizon of low $\delta^{13}C$ of *N. pachyderma* (s.) and changes in the absolute abundance of *N. labradorica* at both sites during several events. These correlations are highly statistically significant (Table 4), and are consistent with the interpretation that each layer of authigenic carbonates is associated with periods of strongly elevated methane flux from the subsurface to shallow sediments.

[45] This relationship between the occurrence of authigenic carbonates and changes in benthic foraminiferal abundance is weaker in 57JPC than in 51JPC. However, site 57JPC is within the oxygen minimum zone (OMZ), and the position and intensity of the OMZ strongly influences benthic fauna (see review by *Bernhard and Sen Gupta* [1999]). Both OMZ and seep fauna are quite variable, but both include species that are adapted to low-oxygen and sulfidic environments. Site 51JPC is well below the OMZ, so we would not expect the benthic faunal abundance to be overprinted by the OMZ as in 57JPC.

[46] The correlation between the authigenic-carbonate-rich layers and abundance of benthic foraminifera is weaker in 57JPC at 368–392 cm, 464–480 cm. Since we did not study the biomarkers at high resolution for these episodes, we cannot rule out the possibility that in this core, these horizons could be related to strong vertical methane flux but not to methane seepage at the seafloor. However, considering the persistent relationship between the benthic foraminiferal abundance and authigenic carbonates in 51JPC, a site far from the influence of the OMZ, it is possible that in 57JPC the methane flux also reached the seafloor, but was poorly recorded in the benthic foraminiferal abundances. Therefore, the abundance and species distribution of benthic foraminifera provide strong evidence that the authigenic carbonates are a record of methane flux to the shallow sediments, or to the seafloor, rather than deep in the subsurface.

4.3. Climate Implications

[47] The radiocarbon-based age model allows us to date the three most recent authigenic-carbonate-rich horizons (Figure 6). These horizons are 2 m shallower in 57JPC than in 51JPC, but within the uncertainty of the age model, they are contemporaneous in the two sediment cores. The uncertainty in the calibrated radiocarbon dates at 25 ka is 340–410 years (1σ), so it is not possible to analyze phasing of the events between the two cores. However, assuming the authigenic-carbonate-rich layers were each formed at approximately the same depth range below the seafloor, we can calculate that the three episodes of low $\delta^{13}C$ were spaced slightly greater than 1000 years apart. This is similar to timing of D-O events, and we observe no events in either core between 22 and 15 ka, a time when D-O events did not occur either. Based on the timing of events between the two cores and the similarity in the isotopic signature of the

excursions, we hypothesize that these horizons each formed during region-wide episodes of high methane flux, and that these episodes are linked to the climate and ocean circulation changes during D-O events.

[48] Each ^{13}C-depleted authigenic-carbonate-rich horizon unambiguously represents episodes of enhanced vertical methane flux during the last glacial period at times of known millennial-scale climate changes. This supports the idea [*Kennett et al.*, 2003], that sedimentary methane interacts with the climate system on these timescales. However, both coring sites are cold and deep, and destabilization of methane hydrates would require an unrealistic warming (6–16°C) or sea level drop (300–1000 m) (Figure S1).

[49] Simulations of the response of methane hydrates to temperature changes shows that with as little as 1°C warming, shallow deposits can undergo rapid dissociation and produce significant methane fluxes within decades [*Reagan and Morodis*, 2007]. For deep deposits (>1000 m water depth), temperature change of up to 5°C adjusts the top and bottom boundaries of methane hydrate deposits, but does not result in significant methane flux from the seafloor [*Reagan and Morodis*, 2007; *Xu and Lowell*, 2001]. However, even at temperatures and depths where methane hydrates would be thermodynamically stable, methane can be mobilized. For example, (1) the concentration is not high enough to form hydrate, (2) there is a kinetic barrier to hydrate formation [*Brewer et al.*, 1998], or (3) pore water chemistry is altered to prevent hydrate formation [*Liu and Flemings*, 2006]. Examples of active seeps within the methane hydrate stability zone include the Congo Basin and Black Sea [*Charlou et al.*, 2004; *Heeschen et al.*, 2003; *Klaucke et al.*, 2005] and at areas of high fluid flow like the Oregon and Aleutian subduction zones [*Kulm et al.*, 1986; *Suess et al.*, 1998], and at mud volcanoes [*Kopf*, 2002].

[50] In the Bering Sea, fluid flow is strongly influenced by silica diagenesis. Opaline sediments in the Bering Sea reflect the high productivity in the surface waters [*Talley and Joyce*, 1992]. Productivity is particularly high in a belt along the Bering Slope and along the Aleutian Islands [*Springer et al.*, 1996] and the Umnak Plateau is at the juncture of these two zones. When diatom-rich sediments are buried and undergo compaction, the opal-A (biogenic silica) turns into opal-CT (cristobalite and tridymite). This diagenetic dehydration reaction causes a decrease in porosity of the sediment and expulsion of water from the crystal matrix that result in elevated pore fluid pressure and upward fluid flow over large areas [*Davies et al.*, 2008] or focused fluid flow in sediment [*Davies and Clark*, 2006].

[51] The opal-A to opal-CT diagenetic front is seen as a bottom simulating reflector in the Umnak Plateau region at 670 m below the seafloor at the transition between terrigenous-rich, diatomaceous sediments (average 65% diatoms) to siltstone [*Scholl et al.*, 1973]. Silica diagenesis could result in a buildup of overpressure that is accompanied by a decrease in the shear strength of sediment, priming it for failure. The exfoliation of submarine canyons driven by high pore fluid pressures is an important mechanism in shaping the canyons on the Bering Slope [*McHugh et al.*, 1993], including Bristol and Bering canyons, between which our study area lies.

[52] In this study, we see a similar pattern of methane seepage at two different sites. This is consistent with large-scale regional fluid flow. Since the isotopic composition of the authigenic carbonates appears similar not only between each episode but also between the two coring areas (Figure 4), it suggests that the methane flux could have been operating over the entire region, drawing from a common reservoir of methane-laden fluids, resulting in similar conditions during episodes. Since the microbial biomass is dominated by sedimentary anaerobic methanotrophic communities, and there is no sign of aerobic methanotrophs, it is unlikely that catastrophic release of methane into the water column was the dominant mechanism. However, elevated methane flux on a regional scale could have resulted in methane release into the water column.

[53] What would have caused episodic methane flux in the past? One way to relieve overpressure in pore fluids is through seismic shaking. The Umnak Plateau lies between the Aleutian trench, an active subduction zone, and the Bering Slope, the position of the subduction zone in the Tertiary [*Cooper et al.*, 1976], and which is associated with many relict faults. Seismic shaking could produce widespread, elevated fluid flow, as was observed following slow earthquakes on the Costa Rican margin [*Brown et al.*, 2005]. This is consistent with the moderate AOM rates implied by the inferred ANME-1 consortium and the stable isotope and radiocarbon estimates of the authigenic carbonates. Gas and methane-rich fluids could also travel rapidly upward along fault planes or laterally along bedding planes that intersect a fault, forming seeps at the seafloor. These locations could release methane rapidly to the water column, and with high enough flux could potentially influence the atmospheric methane budget.

[54] If seismic shaking is the main way that overpressured pore fluids were released in the past, what controls the frequency of the episodes of fluid and gas release? We speculate that changes in the water column have the potential to have caused methane mobilization in the southeast Bering Sea during the last glacial period. The slip associated with slow earthquakes in subduction zones around the rim of the Pacific are observed to be periodic, and have been linked to the 14 month pole tide [*Lowry*, 2006; *Shen et al.*, 2005]. A small hydrostatic pressure change of ~160 Pa occurs on the subduction zones when the pole tide passes overhead, resulting in Coulomb failure, slow slip, and low-frequency shaking [*Shen et al.*, 2005]. During the last glacial period, changes in ocean circulation and sea level [*Siddall et al.*, 2003] occurred with the Dansgaard-Oeschger climate events. Sea level increased by up to 35 m at the beginning of the warm climate events, with rates of rise of up to 2 cm per year [*Siddall et al.*, 2003].

[55] We speculate that the sediments of the southeast Bering Sea could be primed for rapid methane and fluid release by the overpressure of pore fluids by silica diagenesis. With sea level rise at the beginning of a Dansgaard-Oeschger event, the hydrostatic pressure change on the Aleutian subduction zone could have triggered seismic shaking. The shaking could have caused region-wide upward fluid flow and rapid expulsion of methane and methane bearing pore fluids along faults and bedding planes, inducing near-surface AOM with associated precipitation of authigenic carbonate minerals. During the stadials, the continuing silica diagenesis would then repressurize the pore fluids.

[56] To test this mechanism would require hydrogeological modeling, including methanogenesis, compaction, silica diagenesis (to determine the magnitude of overpressure that could be generated in 1 to 4 kyr), and estimation of the amount of methane that could be mobilized by a fluid expulsion episode. In addition, modeling of the stress field of the Aleutian subduction zone could test whether hydrostatic pressure changes of the magnitude that occurred during MIS3 could have caused earthquakes.

5. Conclusions

[57] In two sediment cores from the Bering Sea, ^{13}C-depleted authigenic carbonates coincide with ^{13}C-depleted molecular biomarkers indicative of AOM communities, which testify to the existence of repeated pulses of increased vertical flux of methane. In the most recent of the events, the relatively intense biomarker signals provide strong evidence for high methane flux at the shallow subsurface. The lack of signals from aerobic methanotrophic bacteria, on the other hand, argues against catastrophic methane release into the water column at this time. Closely linked to the episodic methane pulses were changes in benthic foraminiferal abundances and species distribution. The mobilization of methane was not related to destabilization of hydrates, since the water depth of the Bering Sea sites are too deep. Alternatively, enhanced fluid flow as a result of silica diagenesis is a mechanism that could result in massive, regional-scale flux of methane bearing pore fluids in this study area, in response to changes in ocean circulation or sea level.

[58] **Acknowledgments.** The success of the HLY02-02 expedition is thanks to the efforts of the science party and crew of the USCGC *Healy*. Mary Carman, Sean Sylva, Carl Johnson, and Xavier Prieto Mollar assisted in sample preparation and analysis. Discussions with Marcus Elvert, Achim Kopf, Carolyn Ruppel, and Daniel Lizzaralde were very helpful during this project. Support for this project was from the National Science Foundation Office of Polar Programs, United States Department of Energy, Oak Foundation, and MARUM at University of Bremen. We thank three anonymous reviewers whose comments significantly improved this manuscript.

References

Aharon, P., et al. (1997), Radiometric dating of submarine hydrocarbon seeps in the Gulf of Mexico, *Geol. Soc. Am. Bull.*, *109*(5), 568–579, doi:10.1130/0016-7606(1997)109<0568:RDOSHS>2.3.CO;2.

Aloisi, G., et al. (2002), Methane-consuming microorganisms and the formation of carbonate crusts at cold seeps, *Earth Planet. Sci. Lett.*, *203*, 195–203, doi:10.1016/S0012-821X(02)00878-6.

Archer, D. E. (2009), Ocean methane hydrates as a slow tipping point in the global carbon cycle, *Proc. Natl. Acad. Sci. U. S. A.*, *106*(49), 20,596–20,601, doi:10.1073/pnas.0800885105.

Bernhard, J. M. (1988), Postmortem vital staining in benthic foraminifera: Duration and importance in population and distributional studies, *J. Foraminiferal Res.*, *18*(2), 143–146, doi:10.2113/gsjfr.18.2.143.

Bernhard, J. M., and B. K. Sen Gupta (1999), Foraminifera of oxygen-depleted environments, in *Modern Foraminifera*, edited by B. K. Sen Gupta, pp. 201–216, Kluwer Acad., Dordrecht, Netherlands.

Bernhard, J. M., et al. (2001), Monterey Bay cold-seep biota: Assemblages, abundance, and ultrastructure of living foraminifera, *Deep Sea Res., Part I*, *48*, 2233–2249, doi:10.1016/S0967-0637(01)00017-6.

Bernstein, B. B., et al. (1978), Spatial dispersion of benthic foraminifera in the abyssal central North Pacific, *Limnol. Oceanogr.*, *23*(3), 401–416, doi:10.4319/lo.1978.23.3.0401.

Bhaumik, A. K., and A. K. Gupta (2007), Evidence of methane release from Blake Ridge: ODP Hole 997A during the Plio-Pleistocene: Benthic foraminifer fauna and total organic carbon, *Curr. Sci.*, *92*(2), 192–199.

Bian, L., et al. (2001), Algal and archael polyisoprenoides in a recent marine sediment: Molecular isotopic evidence for anaerobic oxidation of methane, *Geochem. Geophys. Geosyst.*, *2*, 1023, doi:10.1029/2000GC000112.

Biddle, J. F., et al. (2006), Heterotrophic archaea dominate sedimentary subsurface ecosystems off Peru, *Proc. Natl. Acad. Sci. U. S. A.*, *103*(10), 3846–3851, doi:10.1073/pnas.0600035103.

Blumenberg, M., et al. (2004), Membrane lipid patterns typify distinct anaerobic methanotropic consortia, *Proc. Natl. Acad. Sci. U. S. A.*, *101*(30), 11,111–11,116, doi:10.1073/pnas.0401188101.

Blunier, T., and E. J. Brook (2001), Timing of millennial-scale climate change in Antarctica and Greenland during the last glacial period, *Science*, *291*, 109–112, doi:10.1126/science.291.5501.109.

Blunier, T., et al. (1998), Asynchrony of Antarctic and Greenland climate change during the last glacial period, *Nature*, *394*, 739–743, doi:10.1038/29447.

Bock, M., et al. (2010), Hydrogen isotopes preclude marine hydrate CH_4 emissions at the onset of Dansgaard-Oeschger events, *Science*, *328*, 1686–1689, doi:10.1126/science.1187651.

Borowski, W. S., et al. (1996), Marine pore-water sulfate profiles indicate in situ methane flux from underlying gas hydrate, *Geology*, *24*(7), 655–658, doi:10.1130/0091-7613(1996)024<0655:MPWSPI>2.3.CO;2.

Brewer, P. G., et al. (1998), Gas hydrate formation in the deep sea: In situ experiments with controlled release of methane, natural gas and carbon dioxide, *Energy Fuels*, *12*, 183–188, doi:10.1021/ef970172q.

Brown, K. M., et al. (2005), Correlated transient fluid pulsing and seismic tremor in the Costa Rica subduction zone, *Earth Planet. Sci. Lett.*, *238*(1–2), 189–203, doi:10.1016/j.epsl.2005.06.055.

Brunelle, B. G., D. M. Sigman, M. S. Cook, L. D. Keigwin, G. H. Haug, B. Plessen, G. Schettler, and S. L. Jaccard (2007), Evidence from diatom-bound nitrogen isotopes for subarctic Pacific stratification during the last ice age and a link to North Pacific denitrification changes, *Paleoceanography*, *22*, PA1215, doi:10.1029/2005PA001205.

Chappellaz, J., et al. (1990), Ice-core record of atmospheric methane over the past 160,000 years, *Nature*, *345*, 127–131, doi:10.1038/345127a0.

Charlou, J. L., et al. (2004), Physical and chemical characterization of gas hydrates and associated methane plumes in the Congo-Angola Basin, *Chem. Geol.*, *205*(3–4), 405–425, doi:10.1016/j.chemgeo.2003.12.033.

Claypool, G. E., et al. (1973), Gas analyses in sediment samples from Legs 10, 11, 13, 14, 15, 18, and 19, *Initial Rep. Deep Sea Drill. Proj.*, *19*, 879–884.

Cook, M. S., et al. (2005), The deglacial history of surface and intermediate water of the Bering Sea, *Deep Sea Res., Part II*, *52*, 2163–2173, doi:10.1016/j.dsr2.2005.07.004.

Cooper, A. K., et al. (1976), Plate tectonic model for the evoluion of the eastern Bering Sea Basin, *Geol. Soc. Am. Bull.*, *87*(8), 1119–1126, doi:10.1130/0016-7606(1976)87<1119:PTMFTE>2.0.CO;2.

Davies, R. J., and I. R. Clark (2006), Submarine slope failure primed and triggered by silica and its diagenesis, *Basin Res.*, *18*, 339–350, doi:10.1111/j.1365-2117.2006.00297.x.

Davies, R. J., et al. (2008), Fluid flow due to the advance of basin-scale silica reaction zones, *Geol. Soc. Am. Bull.*, *120*(1–2), 195–206, doi:10.1130/B26099.1.

de Garidel-Thoron, T., et al. (2004), Evidence for large methane releases to the atmosphere from deep-sea gas-hydrate dissociation during the last glacial episode, *Proc. Natl. Acad. Sci. U. S. A.*, *101*(25), 9187–9192, doi:10.1073/pnas.0402909101.

Dickens, G. R., J. R. O'Neil, D. K. Rea, and R. M. Owen (1995), Dissociation of oceanic methane hydrate as a cause of the carbon isotope excursion at the end of the Paleocene, *Paleoceanography*, *10*(6), 965–971, doi:10.1029/95PA02087.

Fritz, P., and D. G. W. Smith (1970), The isotopic composition of secondary dolomites, *Geochim. Cosmochim. Acta*, *34*, 1161–1173, doi:10.1016/0016-7037(70)90056-6.

Godwin, H. (1962), Half-life of radiocarbon, *Nature*, *195*, 984, doi:10.1038/195984a0.

Greinert, J., et al. (2002), Stromatolitic fabric of authigenic carbonate crusts: Result of anaerobic methane oxidation at cold seeps in 4850 m water depth, *Int. J. Earth Sci.*, *91*, 698–711, doi:10.1007/s00531-001-0244-9.

Heeschen, K. U., A. M. Tréhu, R. W. Collier, E. Suess, and G. Rehder (2003), Distribution and height of methane bubble plumes on the Cascadia Margin characterized by acoustic imaging, *Geophys. Res. Lett.*, *30*(12), 1643, doi:10.1029/2003GL016974.

Heinz, P., et al. (2005), Living benthic foraminifera in sediments influenced by gas hydrates at the Cascadia convergent margin, NE Pacific, *Mar. Ecol. Prog. Ser.*, *304*, 77–89, doi:10.3354/meps304077.

Hesselbo, S. P., et al. (2000), Massive dissociation of gas hydrate during a Jurassic ocean anoxic event, *Nature*, *406*, 392–395, doi:10.1038/35019044.

Hill, T. M., et al. (2004), Isotopic evidence for the incorporation of methane-derived carbon into foraminifera from modern methane seeps, Hydrate

Ridge, Northeast Pacific, *Geochim. Cosmochim. Acta*, *68*, 4619–4627, doi:10.1016/j.gca.2004.07.012.
Hill, T. M., et al. (2006), Climatically driven emissions of hydrocarbons from marine sediments during deglaciation, *Proc. Natl. Acad. Sci. U. S. A.*, *103*(37), 13,570–13,574, doi:10.1073/pnas.0601304103.
Hinrichs, K.-U. (2001), A molecular recorder of methane hydrate destabilization, *Geochem. Geophys. Geosyst.*, *2*, 1029, doi:10.1029/2000GC000118.
Hinrichs, K.-U., et al. (2000), Molecular and isotopic analysis of anaerobic methane-oxidizing communities in marine sediments, *Org. Geochem.*, *31*, 1685–1701, doi:10.1016/S0146-6380(00)00106-6.
Hinrichs, K.-U., et al. (2003), Molecular fossil record of elevated methane levels in late Pleistocene coastal waters, *Science*, *299*, 1214–1217, doi:10.1126/science.1079601.
Hoefs, M. J. L., et al. (1997), Ether lipids of planktonic archaea in the marine water column, *Appl. Environ. Microbiol.*, *63*(8), 3090–3095.
Hoshiba, M., et al. (2006), Foraminiferal oxygen and carbon isotopes during the last 34 kyr off northern Japan, northwestern Pacific, *Mar. Micropaleontol.*, *61*, 196–208, doi:10.1016/j.marmicro.2006.07.001.
Johnsen, S. J., et al. (1992), Irregular glacial interstadials recorded in a new Greenland ice core, *Nature*, *359*, 311–313, doi:10.1038/359311a0.
Johnsen, S. J., et al. (2001), Oxygen isotope and palaeotemperature records from six Greenland ice-core stations: Camp Century, Dye-3, GRIP, GISP2, Reland and NorthGRIP, *J. Quaternary Sci.*, *16*(4), 299–307, doi:10.1002/jqs.622.
Judd, A. G. (2000), Geological sources of methane, in *Atmospheric Methane: Its Role in the Global Environment*, edited by M. Khalil, pp. 280–303, Springer, New York.
Keigwin, L. D. (2002), Late Pleistocene-Holocene paleoceangraphy and ventilation of the Gulf of California, *J. Oceanogr.*, *58*, 421–432, doi:10.1023/A:1015830313175.
Kennett, J. P., et al. (2000), Carbon isotopic evidence for methane hydrate instability during Quaternary interstadials, *Science*, *288*, 128–133, doi:10.1126/science.288.5463.128.
Kennett, J. P., K. G. Cannariato, I. L. Hendy, and R. J. Behl (2003), *Methane Hydrates in Quaternary Climate Change: The Clathrate Gun Hypothesis*, *Spec. Publ. Ser.*, vol. 54, AGU, Washington, D. C.
Kessler, J. D., W. S. Reeburgh, D. L. Valentine, F. S. Kinnaman, E. T. Peltzer, P. G. Brewer, J. Southon, and S. C. Tyler (2008), A survey of methane isotope abundance (^{14}C, ^{13}C, ^{2}H) from five nearshore marine basins that reveals unusual radiocarbon levels in subsurface waters, *J. Geophys. Res.*, *113*, C12021, doi:10.1029/2008JC004822.
Kim, S.-T., and J. R. O'Neil (1997), Equilibrium and nonequilibrium oxygen isotope effects in synthetic carbonates, *Geochim. Cosmochim. Acta*, *61*(16), 3461–3475, doi:10.1016/S0016-7037(97)00169-5.
Kim, S.-T., J. R. O'Neil, A. Mucci, and C. Hillaire-Marcel (2004), Oxygen isotope fractionation between synthetic aragonite and water: Influence of solution chemistry, *Eos Trans. AGU*, *85*(47), Fall Meeting Suppl., Abstract V51C-0589.
Klaucke, I., W. Weinrebe, H. Sahling, G. Bohrmann, and D. Bürk (2005), Mapping deep-water gas emissions with sidescan sonar, *Eos Trans. AGU*, *86*(38), 341, doi:10.1029/2005EO380002.
Koga, Y., and M. Nakano (2008), A dendogram of archaea based on lipid component parts composition and its relationship to rRNA phylogeny, *Syst. Appl. Microbiol.*, *31*(3), 169–182, doi:10.1016/j.syapm.2008. 02.005.
Kopf, A. J. (2002), Significance of mud volcanism, *Rev. Geophys.*, *40*(2), 1005, doi:10.1029/2000RG000093.
Kulm, L. D., et al. (1986), Oregon subduction zone: Venting, fauna and carbonates, *Science*, *231*(4738), 561–566, doi:10.1126/science.231.4738.561.
Leifer, I., B. P. Luyendyk, J. Boles, and J. F. Clark (2006), Natural marine seepage blowout: Contribution to atmospheric methane, *Global Biogeochem. Cycles*, *20*, GB3008, doi:10.1029/2005GB002668.
Lelieveld, J., et al. (1993), Climate effecs of atmospheric methane, *Chemosphere*, *26*(1–4), 739–768, doi:10.1016/0045-6535(93)90458-H.
Lembke, L., R. Tiedemann, D. Nürnberg, N. Biebow, and A. Kaiser (2004), Benthic foraminiferal C-13 anomalies in the Okhotsk Sea: Evidence for Holocene methane dissociation events, *Eos Trans. AGU*, *85*(17), Jt. Assem. Suppl., Abstract 10976.
Lipp, J. S., and K.-U. Hinrichs (2009), Structural diversity and fate of intact polar lipids in marine sediments, *Geochim. Cosmochim. Acta*, *73*(22), 6816–6833, doi:10.1016/j.gca.2009.08.003.
Liu, X., and P. B. Flemings (2006), Passing gas through the hydrate stability zone at southern Hydrate Ridge, offshore Oregon, *Earth Planet. Sci. Lett.*, *241*(1–2), 211–226, doi:10.1016/j.epsl.2005.10.026.
Loulergue, L., et al. (2008), Orbital and millennial-scale features of atmospheric CH_4 over the past 800,000 years, *Nature*, *453*, 383–386, doi:10.1038/nature06950.
Lowry, A. R. (2006), Resonant slow fault slip in subduction zones forced by climatic load stress, *Nature*, *442*, 802–805, doi:10.1038/nature05055.
Maslin, M., et al. (1998), Sea-level- and gas-hydrate-controlled catastrophic sediment failures of the Amazon Fan, *Geology*, *26*(12), 1107–1110, doi:10.1130/0091-7613(1998)026<1107:SLAGHC>2.3.CO;2.
Maslin, M., et al. (2005), Causes of catastrophic sediment failures of the Amazon Fan, *Quat. Sci. Rev.*, *24*, 2180–2193, doi:10.1016/j.quascirev.2005.01.016.
Matsumoto, R., and W. S. Borowski (2000), Gas hydrate estimates from newly determined oxygen isotopic fractionation (alpha-GH-IW) and $\delta^{18}O$ anomalies of the interstitial waters: Leg 164, Blake Ridge, *Proc. Ocean Drill. Program Sci. Results*, *164*, 59–66.
McGinnis, D. F., J. Greinert, Y. Artemov, S. E. Beaubien, and A. Wüest (2006), Fate of rising methane bubbles in stratified waters: How much methane reaches the atmosphere?, *J. Geophys. Res.*, *111*, C09007, doi:10.1029/2005JC003183.
McHugh, C. M., et al. (1993), The role of diagenesis in exfoliation of submarine canyons, *Am. Assoc. Pet. Geol. Bull.*, *77*(2), 145–172.
Ménot, G., and E. Bard (2010), Geochemical evidence for a large methane release during the last deglaciation from Marmara Sea sediments, *Geochim. Cosmochim. Acta*, *74*, 1537–1550, doi:10.1016/j.gca.2009.11.022.
Millo, C., et al. (2005), Methane-driven late Pleistocene $\delta^{13}C$ minima and overflow reversals in the southwestern Greenland Sea, *Geology*, *33*(11), 873–876, doi:10.1130/G21790.1.
Naehr, T. H., et al. (2009), Biogeochemical controls on authigenic carbonate formation at the Chapopote "asphalt volcano", Bay of Campeche, *Chem. Geol.*, *266*(3–4), 390–402, doi:10.1016/j.chemgeo.2009.07.002.
Niemann, H., and M. Elvert (2008), Diagnostic lipid biomarker and stable carbon isotope signatures of microbial communities mediating the anaerobic oxidation of methane with sulphate, *Org. Geochem.*, *39*(12), 1668–1677, doi:10.1016/j.orggeochem.2007.11.003.
Niemann, H., et al. (2005), Methane emission and consumption at a North Sea gas seep (Tommeliten area), *Biogeosci. Discuss.*, *2*, 1197–1241, doi:10.5194/bgd-2-1197-2005.
Orphan, V. J., et al. (2004), Geological, geochemical, and microbiological heterogeneity of the seafloor around methane vents in the Eel River Basin, offshore California, *Chem. Geol.*, *205*, 265–289, doi:10.1016/j.chemgeo.2003.12.035.
Ostermann, D. R., and W. B. Curry (2000), Calibration of stable isotopic data: An enriched $\delta^{18}O$ standard used for source gas mixing detection and correction, *Paleoceanography*, *15*(3), 353–360, doi:10.1029/1999PA000411.
Peckmann, J., and V. Thiel (2004), Carbon cycling at ancient methane seeps, *Chem. Geol.*, *205*(3–4), 443–467, doi:10.1016/j.chemgeo.2003.12.025.
Peckmann, J., et al. (2001), Methane-derived carbonates and authigenic pyrite from the northwestern Black Sea, *Mar. Geol.*, *177*, 129–150, doi:10.1016/S0025-3227(01)00128-1.
Petrenko, V. V., et al. (2009), $^{14}CH_4$ measurements in Greenland ice: Investigating last glacial termination CH_4 sources, *Science*, *324*, 506–508, doi:10.1126/science.1168909.
Rathburn, A. E., et al. (2000), Benthic foraminifera associated with cold methane seeps on the northern California margin: Ecology and stable isotopic composition, *Mar. Micropaleontol.*, *38*, 247–266, doi:10.1016/S0377-8398(00)00005-0.
Reagan, M. T., and G. J. Morodis (2007), Oceanic gas hydrate instability and dissociation under climate change scenarios, *Geophys. Res. Lett.*, *34*, L22709, doi:10.1029/2007GL031671.
Reeburgh, W. S. (2007), Oceanic methane biogeochemistry, *Chem. Rev.*, *107*, 486–513, doi:10.1021/cr050362v.
Reimer, P. J., et al. (2009), IntCal09 and Marine09 radiocarbon age calibration curves, 0–50,000 years cal BP, *Radiocarbon*, *51*(4), 1111–1150.
Rossel, P. E., et al. (2008), Intact polar lipids of anaerobic methanotropic archaea and associated bacteria, *Org. Geochem.*, *39*(8), 992–999, doi:10.1016/j.orggeochem.2008.02.021.
Schaefer, H., et al. (2006), Ice record of $\delta^{13}C$ for atmospheric CH_4 across the Younger Dryas-Preboreal transition, *Science*, *313*, 1109–1112, doi:10.1126/science.1126562.
Schmidt, M., et al. (2002), Seeping hydrocarbons and related carbonate mineralisations in sediments south of Lihir Island (New Ireland forearc basin, Paupua New Guinea), *Chem. Geol.*, *186*, 249–264, doi:10.1016/S0009-2541(01)00419-3.
Scholl, D. W., et al. (1973), Site 185, *Initial Rep. Deep Sea Drill. Proj.*, *19*, 169–216.
Schouten, S., et al. (1998), Structural characterization, occurrence and fate of archael ether-bound acyclic biphytanes and corresponding diols in sediments, *Org. Geochem.*, *29*(5–7), 1305–1319, doi:10.1016/S0146-6380(98)00131-4.
Schouten, S., et al. (2002), Distributional variations in marine crenarchaeotal membrane lipids: A noew tool for reconstructing ancient seawater temperatures?, *Earth Planet. Sci. Lett.*, *204*, 265–274, doi:10.1016/S0012-821X(02)00979-2.

Shen, Z.-K., et al. (2005), Pole-tide modulation of slow slip events at circum-Pacific subduction zones, *Bull. Seismol. Soc. Am.*, *95*(5), 2009–2015, doi:10.1785/0120050020.

Siddall, M., et al. (2003), Sea-level fluctuations during the last glacial cycle, *Nature*, *423*, 853–858, doi:10.1038/nature01690.

Sinninghe Damasté, J. S., et al. (2002), Linearly concatenated cyclobutane lipids form a dense bacterial membrane, *Nature*, *419*, 708–712, doi:10.1038/nature01128.

Smith, W. H. F., and D. T. Sandwell (1997), Global sea floor topography from satellite altimetry and ship depth soundings, *Science*, *277*(5334), 1956–1962, doi:10.1126/science.277.5334.1956.

Smith, L. M., J. P. Sachs, A. E. Jennings, D. M. Anderson, and A. deVernal (2001), Light $\delta^{13}C$ events during deglaciation of the East Greenland Continental Shelf attributed to methane release from gas hydrates, *Geophys. Res. Lett.*, *28*(11), 2217–2220, doi:10.1029/2000GL012627.

Solomon, E. A., et al. (2009), Considerable methane fluxes to the atmosphere from hydrocarbon seeps in the Gulf of Mexico, *Nat. Geosci.*, *2*, 561–565, doi:10.1038/ngeo574.

Solomon, S., D. Qin, M. Manning, Z. Chen, M. Marquis, K. Averyt, M. Tignor, and H. Miller (Eds.) (2007), *Climate Change 2007: The Physical Science Basis: Contribution of Working Group I to the Fourth Assessment Report on the Intergovernmental Panel on Climate Change*, Cambridge Univ. Press, Cambridge, U. K.

Sowers, T. (2006), Late Quaternary atmospheric CH_4 isotope record suggests marine clathrates are stable, *Science*, *311*, 838–840, doi:10.1126/science.1121235.

Springer, A. M., et al. (1996), The Bering Sea Green Belt: Shelf-edge processes and ecosystem production, *Fish. Oceanogr.*, *5*(3–4), 205–223, doi:10.1111/j.1365-2419.1996.tb00118.x.

Stuiver, M., and P. J. Reimer (1993), Extended ^{14}C data base and revised CALIB 3.0 ^{14}C age calibration program, *Radiocarbon*, *35*(1), 215–230.

Suess, E., et al. (1998), Fluid venting in the eastern Aleutian subduction zone, *J. Geophys. Res.*, *103*(B2), 2597–2614, doi:10.1029/97JB02131.

Summons, R. E., et al. (1994), Carbon isotopic fractionation in lipids from methanotrophic bacteria: Relevance for interpretation of the geochemical record of biomarkers, *Geochim. Cosmochim. Acta*, *58*(13), 2853–2863, doi:10.1016/0016-7037(94)90119-8.

Takahashi, K., A. C. Ravelo, C. A. Alvarez Zarikian, and the Expedition 323 Scientists (2011), *Bering Sea Paleoceanography*, *Proc. Integr. Ocean Drill. Program*, *323*, doi:10.2204/iodp.proc.323.2011.

Talley, L. D., and T. M. Joyce (1992), The double silica maximum in the North Pacific, *J. Geophys. Res.*, *97*(C4), 5465–5480, doi:10.1029/92JC00037.

Tarutani, T., et al. (1969), The effect of polymorphism and magnesium substitution on oxygen isotope fractionation between calcium carbonate and water, *Geochim. Cosmochim. Acta*, *33*, 987–996, doi:10.1016/0016-7037(69)90108-2.

Teske, A., et al. (2002), Microbial diversity of hydrothermal sediments in the Guaymas Basin: Evidence for anaerobic methanotropic communities, *Appl. Environ. Microbiol.*, *68*(4), 1994–2007, doi:10.1128/AEM.68.4.1994-2007.2002.

Torres, M. E., A. C. Mix, K. Kinports, B. Haley, G. P. Klinkhammer, J. McManus, and M. A. de Angelis (2003), Is methane venting at the seafloor recorded by $\delta^{13}C$ of benthic foraminifera shells?, *Paleoceanography*, *18*(3), 1062, doi:10.1029/2002PA000824.

Treude, T., et al. (2005), Anaerobic oxidation of methane and sulfate reduction along the Chilean continental margin, *Geochim. Cosmochim. Acta*, *69*(11), 2767–2779, doi:10.1016/j.gca.2005.01.002.

Uchida, M., Y. Shibata, K. Ohkushi, N. Ahagon, and M. Hoshiba (2004a), Episodic methane release events from Last Glacial marginal sediments in the western North Pacific, *Geochem. Geophys. Geosyst.*, *5*, Q08005, doi:10.1029/2004GC000699.

Uchida, M., Y. Shibata, K. Ohkushi, N. Ahagon, and M. Hoshiba (2004b), Episodic methane release events from Last Glacial marginal sediments in the western North Pacific, *Geochem. Geophys. Geosyst.*, *5*, Q08005, doi:10.1029/2004GC000699.

Uchida, M., K. Ohkushi, K. Kimoto, F. Inagaki, T. Ishimura, U. Tsunogai, T. TuZino, and Y. Shibata (2008), Radiocarbon-based carbon source quantification of anomalous isotopic foraminifera in last glacial sediments in the western North Pacific, *Geochem. Geophys. Geosyst.*, *9*, Q04N14, doi:10.1029/2006GC001558.

Ussler, W., III, and C. K. Paull (2008), Rates of anaerobic oxidation of methane and authigenic carbonate mineralization in methane-rich deep-sea sediments inferred from models and geochemical profiles, *Earth Planet. Sci. Lett.*, *266*(3–4), 271–287, doi:10.1016/j.epsl.2007.10.056.

Valentine, D. L., et al. (2010), Asphalt volcanoes as a potential source of methane to late Pleistocene coastal waters, *Nat. Geosci.*, *3*(5), 345–348, doi:10.1038/ngeo848.

Wakeham, S. G., et al. (2003), Archaea mediate anaerobic oxidation of methane in deep euxinic waters of the Black Sea, *Geochim. Cosmochim. Acta*, *67*(7), 1359–1374, doi:10.1016/S0016-7037(02)01220-6.

Wefer, G., et al. (1994), Clues to ancient methane release, *Nature*, *369*, 282, doi:10.1038/369282a0.

Wegener, G., et al. (2008), Assimilation of methane and inorganic carbon by microbial communities mediating the anaerobic oxidation of methane, *Environ. Microbiol.*, *10*(9), 2287–2298, doi:10.1111/j.1462-2920.2008.01653.x.

Wiedicke, M., and W. Weiss (2006), Stable carbon isotope records of carbonates tracing fossil seep activity off Indonesia, *Geochem. Geophys. Geosyst.*, *7*, Q11009, doi:10.1029/2006GC001292.

Winckler, G., W. Aeschbach-Hertig, J. Holocher, R. Kipfer, I. Levin, C. Poss, G. Rehder, E. Suess, and P. Schlosser (2002), Noble gases and radiocarbon in natural gas hydrates, *Geophys. Res. Lett.*, *29*(10), 1423, doi:10.1029/2001GL014013.

Wuebbles, D. J., and K. Hayhoe (2002), Atmospheric methane and global change, *Earth Sci. Rev.*, *57*, 177–210, doi:10.1016/S0012-8252(01)00062-9.

Xu, W., and R. P. Lowell (2001), Effect of seafloor temperature and pressure variations on methane flux from a gas hydrate layer: Comparison between current and late Pleistocene climate conditions, *J. Geophys. Res.*, *106*(B11), 26,413–26,423, doi:10.1029/2001JB000420.

Zeebe, R. E. (2007), Modeling CO_2 chemistry, $\delta^{13}C$, and oxidation of organic carbon and methane in sediment porewater: Implications for paleo-proxies in benthic foraminifera, *Geochim. Cosmochim. Acta*, *71*, 3238–3256, doi:10.1016/j.gca.2007.05.004.

D. Birgel, Department of Geodynamics and Sedimentology, University of Vienna, Althanstr. 14 (UZA II), A-1090 Vienna, Austria.

M. S. Cook, Geosciences Department, Williams College, 947 Main St., Williamstown, MA 01267, USA. (mea.s.cook@williams.edu)

K.-U. Hinrichs, MARUM-Center for Marine Environmental Sciences, University of Bremen, D-28334 Bremen, Germany.

L. D. Keigwin, Geology and Geophysics Department, MS 8, Woods Hole Oceanographic Institution, Woods Hole, MA 02543, USA.